



Review

# Influence of Binary Ligands in Designing Cesium Lead Halide (CsPbX<sub>3</sub>, X = Cl, Br, I) Perovskite Nanocrystals-Oleic Acid and Oleylamine

Ananthakumar Soosaimanickam \*, Alejandro Saura, Noemi Farinós and Rafael Abargues \*

Institut de Ciència dels Materials (ICMUV), Universitat de València, c/Catedràtic José Beltrán 2, 46980 Paterna, Spain; alejandro.saura@uv.es (A.S.); noemi.farinos@uv.es (N.F.)

\* Correspondence: ananthagc@gmail.com (A.S.); rafael.abargues@uv.es (R.A.)

**Abstract:** The surface chemistry of cesium lead halide perovskite nanocrystals has been elaborately studied in recent years and has proved the critical role of carboxylic acids and amines in the formation and stability of the nanocrystals. Specifically, a slight change in the concentration and ratio of the frequently used oleic acid and oleylamine critically influences the resultant phase and physical properties. Thus, understanding the delicate surface of cesium lead halide perovskite nanocrystals mainly relies on chemical bonding and the dynamic ligand environment of these two organic species. In this aspect, this review summarizes experimental findings about the critical role of oleic acid and oleylamine on the nucleation, growth, stability, phase, and morphology of cesium lead halide perovskite nanocrystals and their effect under different circumstances.

**Keywords:** oleylamine; perovskite nanocrystals; oleic acid; photoluminescent quantum yield; ionic surface



**Citation:** Soosaimanickam, A.; Saura, A.; Farinós, N.; Abargues, R. Influence of Binary Ligands in Designing Cesium Lead Halide (CsPbX<sub>3</sub>, X = Cl, Br, I) Perovskite Nanocrystals-Oleic Acid and Oleylamine. *Nanoenergy Adv.* **2023**, *3*, 376–400. <https://doi.org/10.3390/nanoenergyadv3040019>

Academic Editors: Jaemin Kong and Ya Yang

Received: 21 June 2023

Revised: 2 November 2023

Accepted: 3 November 2023

Published: 15 November 2023



**Copyright:** © 2023 by the authors. Licensee MDPI, Basel, Switzerland. This article is an open access article distributed under the terms and conditions of the Creative Commons Attribution (CC BY) license (<https://creativecommons.org/licenses/by/4.0/>).

## 1. Introduction

Organic-inorganic hybrid perovskite (OIHP) and pure inorganic cesium lead halide perovskite nanocrystals (Cs LHP NCs) possess outstanding optical properties for several kinds of applications [1–4]. In particular, a narrow photoluminescence (PL) spectrum width, tunable optical spectra, and easy synthesis approaches result from Cs LHP NCs (CsPbX<sub>3</sub> NCs, X = Cl, Br, I), positioning them as prominent candidates for optoelectronic applications. Moreover, a tunable bandgap from 1.77 to 3.1 eV is obtained by carefully tuning the halide composition [5]. Figure 1 shows a schematic representation of the surface termination of the CsPbBr<sub>3</sub> NC lattice and a representation of colloidal CsPbX<sub>3</sub> NCs and their PL spectra. Countless articles deal with synthesizing and fabricating Cs LHP thin films using solution-processing methods [6–8]. The high photoluminescence quantum yield (PLQY) of Cs LHP NCs is related to several factors, including the nature of precursors, halide concentration in solution, synthesis methods, organic ligands used in the reaction, and the composition of the finally formed NCs [9–11]. The synthesis of perovskite NCs through solution-processed methods has been accelerated to explore the possibilities of preparing them with different functionalities and morphologies. The ionic Pb-X bond, stronger ionic interaction of Cs<sup>+</sup> ions with a PbX<sub>6</sub> framework, and lower lattice energy result in Cs LHP NCs, which are very sensitive to ligand interaction [12–14]. Because of their ionic nature, the synthesis of LHP NCs in solution is fast, but the kinetics of the formation mechanism are less studied [15–17]. Moreover, the surface properties of Cs LHP NCs differ from the traditional II–VI and IV–VI chalcogenide semiconductor quantum dots (QDs). For example, unlike CdSe or PbS QDs, the surface of the CsPbX<sub>3</sub> NCs is given as [CsPbX<sub>3</sub>] [PbX<sub>2</sub>] {AX}, where A = oleylammonium and X = halides and/or oleate [18]. Irrespective of the defect tolerance, the freshly prepared Cs LHP NCs have surface defects due to the deficiency of Pb<sup>2+</sup> and halide ions. These defects must be passivated with cationic and anionic ligands like aliphatic amines (i.e., oleylamine (OAm)) and carboxylic acids

(i.e., oleic acid (OA)). These organic molecules bind to the surface of Cs LHP NCs, forming a protective layer. In general, ligands play an active role in controlling the size, shape, and polydispersity of NCs. Additionally, they provide stability and rule their surface properties and reactivity. Moreover, the selection of solvents and ligands could influence the reaction rate and growth of the Cs LHP NCs [5,19,20]. It is well known that OA and OAm are suitable for preparing Cs LHP NCs using hot-injection and ligand-assisted reprecipitation (LARP) methods. In the presence of amines and carboxylic acids, the optical properties and phase formation of perovskite NCs are affected. Importantly, the role of carboxylic acids and amines in the structural framework of Cs LHP NCs is being characterized by different spectroscopy techniques by several research groups. Among others, binary ligand system such as oleic acid (OA) and oleylamine (OAm) play a significant role in stabilizing Cs LHP NCs and enhancing their optical properties. The ionized state of these ligands offers multiple roles in providing surface passivation and the dissolution of precursors. Even in NC films, it is important to understand the critical role of OA and OAm to elucidate optoelectronic devices' charge transport and efficiency. Although these two ligands are extensively investigated in preparing traditional semiconductor NCs, understanding their chemistry is essential because of the unique surface properties of Cs LHP NCs. In particular, the binding of OA and OAm to nanocrystals (NCs) is highly susceptible to the solvent used during the purification process. Compared with their interaction with traditional semiconductor NCs, they are more labile on the Cs LHP NCs surface. This is also helpful in the ligand-exchange approach [21] to improve the optical properties and the efficiency of devices like LEDs, solar cells and photodetectors [20,22–25]. There are different strategies used to introduce and eliminate the OA/OAm ligand pair that significantly influence the structural and optical properties of Cs LHP NCs. For instance, an excess of OAm could turn the CsPbBr<sub>3</sub> NCs into the lead-depleted non-luminescent perovskite phase, Cs<sub>4</sub>PbBr<sub>6</sub> [26,27]. Also, the excess of ligands could induce different morphologies in Cs LHP NCs.

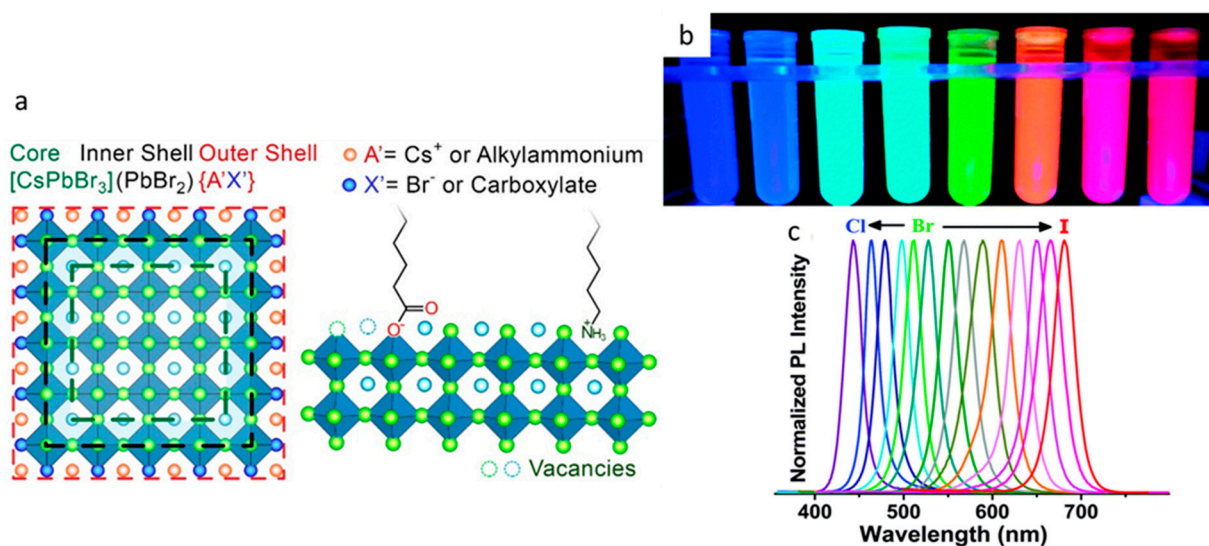


**Figure 1.** (a) Schematic representation of surface termination of a CsPbBr<sub>3</sub> NC lattice. Reprinted from ref. [4]; (b) CsPbX<sub>3</sub> NCs with different emission colors under UV-light illumination; and (c) PL emission spectra of CsPbX<sub>3</sub> NCs with respect to their composition. Reprinted with permission from ref. [15] Copyright© Royal Society of Chemistry.

OA and OAm also direct the self-assembly of NCs to form well-ordered thin films [28,29]. The Bronsted acid–base equilibria between OA and OAm greatly influence the synthesis and assembly of Cs LHP NCs. Also, the presence of these ligands on the NC surface plays a key role in charge transport properties. The inclusion or removal of OA and OAm is useful in tuning the structural and optical properties of the Cs LHP NCs. A few research groups

have spectroscopically confirmed the specific attachment and structural transformation of Cs LHP NCs under the influence of OA and OAm [30,31]. On one hand, these ligands show excellent surface capping properties due to their large size. On the other hand, large ligands strongly hinder the charge transport properties in NC films. Therefore, a common approach used in chalcogenide QDs to enhance the performance of optoelectronic devices is to carry out a ligand exchange with shorter ligands to improve charge carrier mobility [22,23,32,33]. To understand more about the crucial role of OA and OAm, this review summarizes important contributions rendered by these binary ligands to the growth, physical, and chemical properties of colloiddally synthesized Cs LHP NCs.

## 2. Significance of Oleic Acid (OA) and Oleylamine (OAm) in the Formation and Stabilization of Cs LHP NCs

Capping ligands are essential for synthesizing, growing, stabilizing and fabricating densely packed, structured, super-lattice NC films. Figure 2 shows CsPb(Cl, Br)<sub>3</sub> NC synthesis using hot injection and the ligand-assisted room-temperature precipitation method (LARP). According to Protesescu et al., who first demonstrated the hot-injection synthesis of Cs LHP NCs, OA and OAm are essential for dissolving the precursors and stabilizing the resulting NCs [34]. In the LARP approach, adding OA and OAm enhances the solubility of the precursors up to 50 times in dimethyl formamide (DMF) [5]. Also, to increase the reaction temperature, the concentration of OA/OAm is essential for dissolving PbX<sub>2</sub> [35]. Since ligands play a critical role in the stabilization and properties of any NC, it is essential to know their fundamental role in remodeling the surface of Cs LHP NCs. The reactivity of Cs LHP NCs is much larger than that of II–VI or IV–VI chalcogenide semiconductor NCs. Therefore, the attachment of OA and OAm is more crucial in Cs LHP NCs for improving stability. This is mainly attributed to the extreme ionic character of the LHP NCs. The ionicity (difference in Pauling electronegativity) of Cs–X (~1.9–2.4) and Pb–X (~0.8–1.3) is much larger than that of chalcogenide semiconductors like (Pb/Cd)–(S/Se/Te) (~0.2–0.9) [36]. Higher ionicity in bonds reduces the activation energy required for ion migration within the structure, thereby increasing reactivity values. Here, ligands must be used to minimize reactivity by avoiding ion migration, in which an LHP NC releases or captures species from the environment.

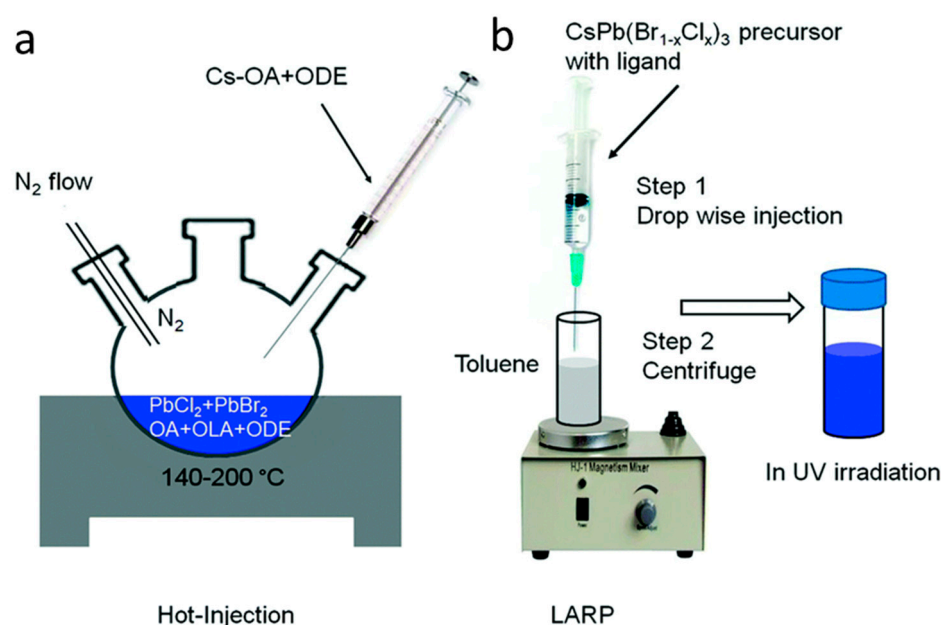
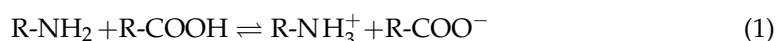


**Figure 2.** Schematic representation of CsPb(Cl, Br)<sub>3</sub> NC synthesis using OAm and OA through (a) hot-injection and (b) the LARP method. Reprinted with permission from ref. [37] Copyright@ Royal Society of Chemistry.

In the hot-injection method, the high-temperature synthesis of Cs LHP NCs is typically carried out in the presence of OAm and OA and a non-coordinating solvent, 1-octadecene (ODE) [37]. Here, a preheated solution of Cs-oleate is injected into the  $\text{PbX}_2/\text{OAm}/\text{OA}$  mixture, and the extremely fast crystallization leads to the formation of Cs LHP NCs. In the LARP method, high-boiling-point solvents (i.e., DMF and dimethyl sulfoxide (DMSO)) are used as solvents of the precursors at room temperature. Here, irrespective of the type of solvents, OAm and OA are commonly used to stabilize NCs, but they have different roles. Generally, OAm enhances the dissolution of precursors and controls the nucleation and growth of NCs in solution, whereas OA avoids the agglomeration of the synthesized NCs [38]. A density functional theory (DFT)-based calculation indicates that the chain length of OA and OAm is estimated as 24.34 and 23.85 Å [39]. This longer chain length of OA/OAm pair greatly influences the structural and morphological properties of Cs LHP NCs.

According to HSAB theory,  $\text{Pb}^{2+}$  is an intermediate Lewis acid, expected to interact with hard bases like oleate ( $\text{OA}^-$ ) and OAm. Therefore, the interaction between  $\text{OA}^-$ , OAm and  $\text{Pb}^{2+}$  results in (1) the direct binding of OAm with  $\text{Pb}^{2+}$  through donating lone-pair electrons from nitrogen, (2) the direct binding of  $\text{OA}^-$  with  $\text{Pb}^{2+}$  to form a Pb-oleate complex, and (3) the formation of Pb-oleate coordination due to the substitution of halides [40]. However, an acid–base reaction between OA and OAm occurs during the synthesis. Here, OAm is protonated to form an oleylammonium cation ( $\text{OAm}^+$ ) and OA deprotonates to form an oleate anion ( $\text{OA}^-$ ), as shown in Equation (1). A dynamic acid–base equilibrium between  $\text{OAm}^+$  and  $\text{OA}^-$  occurs, forming a hydrogen-bond acid–base pair. The equilibrium between OAm and OA can be represented by Equation (1) [27].



Thus, the resulting  $\text{OAm}^+/\text{OA}^-$  ligand pair forms stable colloidal Cs LHP NCs through this dynamic ligand binding effect [38]. In detail, the  $\text{OAm}^+$  binds with surface halides by hydrogen bonding, whereas  $\text{OA}^-$  binds with the uncoordinated surface  $\text{Pb}^{2+}$  or  $\text{Cs}^+$  and forms Pb-O or Cs-O bonds [41]. Later, it was observed that the  $\text{OAm}^+/\text{OA}^-$  ligand pair plays a critical role in controlling the structural and optical properties of Cs LHP NCs. Moreover, the metal–ligand interaction in Cs LHP NCs is not strong enough when OAm and OA ligands are used separately. The experimental results from hot-injection and LARP approaches indicate that only using OA does not lead to the synthesis of Cs LHP NCs. In contrast, employing OAm alone leads to the synthesis of Cs LHP NCs, but these NCs exhibit reduced stability compared to the OA/OAm-capped NCs [42–44].

### 2.1. Structural Modification of Cs LHP NCs Using OA/OAm Ligand Pair

The OAm/OA ligand pair plays an active role in the synthesis and passivation of Cs LHP NCs. The OAm/OA ligand pair can be located between NCs to stabilize the colloids sterically [30,45–47]. However, OAm and OA show a different type of interaction with LHP NCs, which can dramatically affect the LHP stability.  $\text{OAm}^+$  cations can partially replace the  $\text{Cs}^+$  from the structure of Cs LHP NCs or cap the  $\text{Cs}^+$  vacancies to control the phase, morphology, and dimensions of the Cs LHP NCs. Therefore,  $\text{OAm}^+$  can reconstruct  $\text{PbX}_4^{2-}$  octahedra by stabilizing the {110} facet [48], which strongly influences the formation of the perovskite phase [49]. It should be noted that the unprotonated OAm can donate two electrons to the metal center, which also serves for passivation. Moreover, alkylammonium ions can also interact with halide on the surface of the LHP NCs to immobilize them [50]. The concentration of protonated  $\text{OAm}^+$  can be mainly enhanced at lower pH by increasing the concentration of OA [27].

While  $\text{OAm}^+$  substitutes  $\text{Cs}^+$ , the carboxylate group in  $\text{OA}^-$  can bind with  $\text{Pb}^{2+}$  by partially removing the halides [40], leading to a loss of stability. If the deprotonation of OA is hindered, for example, through surface-binding ligands such as ionic liquids, surface passivation is enhanced [51]. Also,  $\text{OAm}^+$  can degrade the NCs by removing lead-oleate from the surface through the formation of an OA/OAm ligand pair [52,53]. Due to the

surface interaction of LHP NCs with the OA/OAm ligand pair being relatively weak, their stability in solution is compromised. Consequently, they exhibit outstanding optical properties over short periods.

Despite the substitution of  $\text{Cs}^+$  ions with incoming  $\text{OAm}^+$  ions, the surface termination of Cs LHP NCs is predominantly associated with the presence of metal halides: either  $\text{PbX}_2$  or  $\text{CsX}$  termination [54]. Through experimental and theoretical model analysis, Ravi et al. proposed that CsBr terminates the surface of the  $\text{CsPbBr}_3$  NCs. Concurrently,  $\text{OAm}^+$  ions also participate in hydrogen bonding interactions with the surface bromide ions [55], as confirmed by X-ray scattering and NMR [56,57]. In general, varying the concentration of OA and OAm drastically alters the optical properties, morphology, and crystalline phase of the Cs LHP NCs. In addition to these, the solubility of  $\text{PbX}_2$  is also affected concerning the concentration of ligands. For example, increasing the concentration of OA/OAm in the reaction enhances the precipitation temperature of  $\text{PbBr}_2$  up to  $290^\circ\text{C}$  [27].

Compared with the mere addition of OA or OAm, the OA/OAm ligand pair improves the PL properties. Here, the dynamic equilibrium between OA and OAm generates a shell around the NCs, which enhances the PL intensity. Interestingly, when a pre-synthesized halide salt of OAm (i.e.,  $\text{OAmBr}$ ) is directly used as a reactant, the resulting  $\text{CsPbBr}_3$  NCs show a near-unity PLQY [9]. Similarly, different kinds of long-chain ammonium halides help to promote the optical properties of Cs LHP NCs [58]. The post-addition of  $\text{OAmBr}$  also alters the morphology and resists the phase transformation of  $\text{CsPbBr}_3$  NCs [59]. It should be noted that the vapor pressure values of OAm and OA are  $\sim 10$  and  $\sim 10^3$  Pa at  $120^\circ\text{C}$ . However, this does not affect the removal or evaporation of these ligands in films [38].

As stated before, spectroscopic observations are indeed helpful in exploring the existence of OA and OAm with Cs LHP NCs. The bonding nature of OA and OAm can be explored through core-loss electron energy loss spectroscopy. Using this method, Kirakosyan et al. found the  $\sigma^*$  peak at 292 eV for the OAm-capped NCs and the  $\pi^*$  feature of the C K-edge of OAm [49]. NMR also helps to identify the interaction of OA/OAm with the Cs LHP NCs. Because of the coordination between ligands, the corresponding resonance appears broader and shifted compared to their spectrum in the free state [54]. Also, the condensation reaction between carboxylic acid and amine results in amide formation, which is detected from the appearance of a peak at  $\delta \sim 3.10$  ppm [60]. The dynamic equilibrium between OA and OAm in Cs LHP NCs is schematically given in Figure 3.

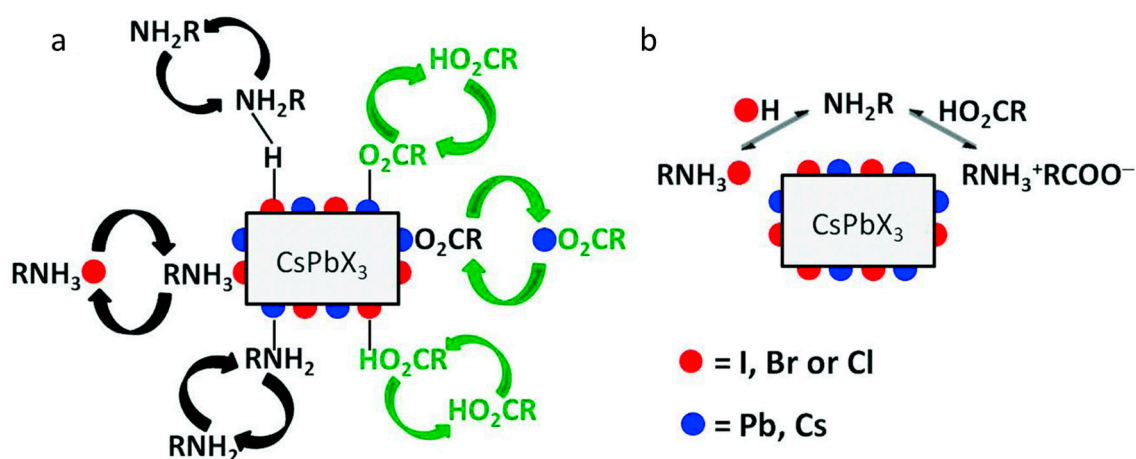


**Figure 3.** (a) Schematic representation of dynamic equilibria between carboxylic acid and amines on the  $\text{CsPbX}_3$  NCs surface. (b) Schematic representation of equilibria of ligands during passivation. Reprinted with permission from ref. [60]. Copyright@ Royal Society of Chemistry.

The interaction of OA/OAm with Cs LHP NCs' surfaces can be detected and confirmed through  $^1\text{H-NMR}$  analysis. The OA/OAm-capped LHP NCs usually show a peak at  $\sim 1.66$  ppm owing to the existence of  $\beta\text{-CH}_2$  groups. The free OAm on the surface reveals an

upfield resonance at  $\delta = 5.55$  ppm, whereas the bonded OAm shows a downfield resonance at  $\delta = 5.68$  ppm [30,49]. The protonation and deprotonation between this ligand pair could be observed from the  $\alpha_1$ -CH<sub>2</sub> <sup>1</sup>H signal at 12.16 ppm. Furthermore, the protonation of OAm by OA and halo acids can be confirmed through the downward shift of the  $\alpha$ -CH<sub>2</sub> resonance in the NMR spectra of the OAm [61].

Figure 4 provides a schematic representation illustrating the modification of OAmBr on the surface of CsPbBr<sub>3</sub> NCs. Additionally, it includes images of the OA/OAm mixture, the chemical structure of oleylammonium oleate, and their respective <sup>1</sup>H-NMR spectra. Although the OA/OAm ligand pair serves as a capping agent, the combination of OA and OAm is also associated with surface Pb<sup>2+</sup> etching when OAm and OA are protonated and deprotonated, respectively. As a result, the acid–base equilibrium in the solution is broken and becomes immobilized within the ligand shell. [49]. Also, OA<sup>−</sup> could coordinate with Pb<sup>2+</sup>, but the reaction kinetics is slower than that of OAm with Pb<sup>2+</sup> [40].

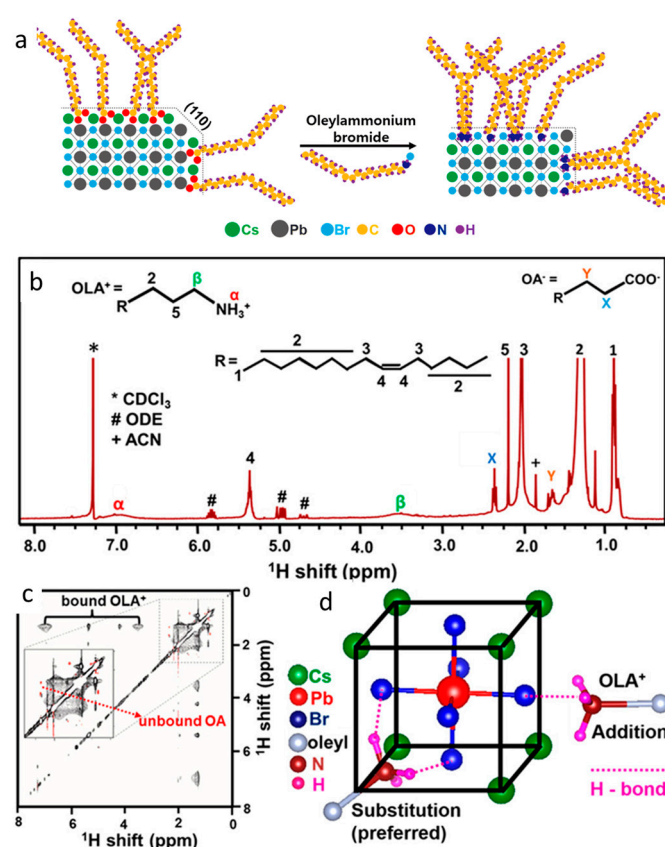


**Figure 4.** (a) Schematic diagram of the interaction of OAmBr with CsPbBr<sub>3</sub> NCs. Reprinted with permission from ref. [59]; (b) <sup>1</sup>H NMR spectrum and (c) Nuclear Overhauser effect spectrum (NOESY) of CsPbBr<sub>3</sub> NCs dispersed in deuterated chloroform; and (d) Schematic diagram of possible binding modes of OAm<sup>+</sup> via hydrogen bond. Reprinted with permission from ref. [55] Copyright 2017 American Chemical Society.

## 2.2. Morphological Changes of Cs LHP NCs in the Presence of OA/OAm

The structural influence of the OA/OAm ligand pair on Cs LHP NCs also leads to the induction of morphological changes. Apart from reaction conditions such as temperature and precursors, the concentration of the OA/OAm ligand pair can produce different morphologies [62]. It is well known that OA and OAm preferentially bind on the Cs-Br and Pb-Br terminated NC surface. The concentration of OA/OAm should be optimal to dissolve the PbBr<sub>2</sub>, but an excess of concentration could dissolve partially Cs LHP NCs [35]. Therefore, it is essential to meticulously control the concentration and ratio of the OA/OAm ligand pair to achieve a narrow distribution of a specific morphology.

For example, upon reaching the optimal concentration of the OA/OAm pair ligand for solubilizing  $\text{PbBr}_2$ , a narrow size distribution of  $\text{CsPbBr}_3$  nanocubes is observed [27]. The competition between  $\text{Cs}^+$  and  $\text{OAm}^+$  dramatically accelerates the growth of Cs LHP NCs with different morphologies. Using halo acids such as HCl, HBr, and HI results in the formation of nanowires (NWs) and nanosheets (NSs) [61,63]. Here, the protonation of OAm by halo acids sterically influences the growth conditions, which direct different morphologies. The advantage of using halo acids is that they can readily supply the halide ions, which react with cationic species. It should be noted that the formation of halo acids also occurs when  $\text{PbX}_2$  reacts with OA, which can also influence the NC morphology. Additionally, the protonation of OAm by halo acid (HBr) slows down the growth of NCs in the vertical direction, which leads to the control of the thickness of the  $\text{CsPbBr}_3$  nanoplatelets (NPLs) [64]. This kind of thickness control in  $\text{CsPbBr}_3$  NPLs has also been achieved by supplying halide (i.e.,  $\text{Br}^-$ ) to the  $\text{OAm}^+$  ions in the presence of benzoyl bromide [65]. Furthermore, with respect to the concentration of halo acids, the phase transformation of  $\text{CsPbBr}_3$  to  $\text{CsPb}_2\text{Br}_5$  is demonstrated [66].

As stated earlier, it is possible to achieve different morphologies of Cs LHP NCs by simply varying the molar ratio of the OA/OAm ligand pair. Li et al. have observed the formation of  $\text{CsPbBr}_3$  NSs with a low amount of OA, whereas the formation of NWs is favored with a high amount of OA [67]. According to the authors, the high presence of OAm disfavors the growth of NCs in the (110) plane, which directs the formation of NPL assembly. In contrast, Almeida et al. have observed the formation of NPLs when the concentration of OA increases [27]. With high OA concentration, the acid–base equilibrium shifts towards OAm protonation, which directs NPL formation [36]. Ji et al. have synthesized  $\text{CsPbBr}_3$  NCs (NSs and NWs) with different morphologies by simply varying the ratio of OA/OAm [68]. Here, uniform NW distribution is achieved using an OA/OAm ratio of 2. Interestingly, Li et al. have synthesized ultrasmall OA/OAm-capped  $\text{CsPbBr}_3$  QDs (~4.5 nm) with high exciton binding energy ( $E_b = 268.7$  meV) using a high OA concentration without 1-ODE [69]. However, by varying the concentration of OA/OAm in the presence of 1-ODE, Liang et al. achieved QDs (2.4 nm) for the ratio 0.6 mL/0.3 mL, whereas NPLs and NSs morphologies were achieved for the ratios 0.5 mL/0.5 mL and 0.2 mL/0.8 mL [70]. Although these investigations deal with the influence of ligands, variation in the reaction temperature could also significantly influence the morphology of Cs LHP NCs. Zhang et al. found that under optimized experimental conditions, the formation of  $\text{CsPbBr}_3$  NWs takes place at 150 °C, whereas over 180 °C is required to synthesize  $\text{CsPbI}_3$  NWs [71]. In this case, with respect to the reaction time, the morphological conversion of  $\text{CsPbBr}_3$  NCs from nanocubes, NWs, NSs and larger size crystals is observed. The formation mechanism of the NWs of Cs LHP NCs consists of different postulates such as dipole-driven attachment, template-directed growth, surfactant-directed growth, seed-mediated growth, etc. Additionally, the modification in morphology can be achieved irrespective of the synthesis method followed. For example, Seth et al. have varied the concentration of OA/OAm to synthesize  $\text{CsPbBr}_3$  NCs in toluene using the LARP method [43]. In this study, it is observed that a higher concentration of OAm (70  $\mu\text{L}$ ) leads to larger nanocubes, whereas a lower concentration (20  $\mu\text{L}$ ) leads to the formation of NR morphology. Interestingly, under prolonged reaction time, these NRs are converted to NWs, which clearly emphasizes the influence of solvents and ligands on morphology transformation. Most of the synthesis protocols of the NWs of Cs LHP NCs are accompanied by OA/OAm ligand pair in the presence of various solvents and ligands. This includes LARP [72], hot injection [71], ultrasonication [73], microfluidic reactor [74], etc. Moreover, this kind of NW can also be achieved through a post-synthetic treatment approach. For example, Yang et al. have achieved ultrathin  $\text{CsPbBr}_3$  NWs (2.5 nm width) by post-synthetically treating  $\text{Cs}_4\text{PbBr}_6$  NCs with  $\text{PbBr}_2$  in short-chain ligands (hexanoic acid, octylamine) [75]. Here, it is proposed that the  $\text{PbBr}_2$ -ligand intermediate, which serves as a lamellar template in the reaction, direct this NWs formation. Similarly, Fanizza et al. have achieved different morphologies of  $\text{CsPbBr}_3$  NCs (nanocubes, NPLs, NWs) through the post-synthetic addition of OA and OAm [76]. Generally, the post-synthetic surface

modification of Cs LHP NCs is influenced by several parameters, such as ligands, the polarity of the solvent, temperature, light, pressure, etc. [77]. The formation of different morphologies of CsPbBr<sub>3</sub> NCs under the post-addition of OA and OAm is schematically provided in Figure 5. Other than this, replacing OA/OAm with short- or long-chain ligands also critically influences the morphology of the Cs LHP NCs [78]. For instance, Pan et al. have modified the chain length of the amine and carboxylic acids in place of OA/OAm in the reaction [31]. In this case, at 170 °C, it was found that decreasing the chain length of carboxylic acids leads to the formation of nanocubes with different sizes, while in the case of amines, NPLs with different thicknesses are achieved. A similar kind of approach using the solvothermal synthesis method (at 100 °C) results in the formation of NWs with different aspect ratios [79]. Along with morphology variation, the thickness of the NWs could be controlled by varying the chain length of the acid/amine in the reaction, which results in NWs with a high PLQY (up to 77%) with significant shifts in the absorption and emission spectra [80]. These results clearly envisage the critical role of the acid/amine pair concerning the morphological variation of Cs LHP NCs. When OA is replaced by a fatty acid—for example, olive oil, the nanocubic morphology of Cs LHP NCs can still be achieved [81]. This is because, at high temperatures, the OA from olive oil produces Cs-oleate and Pb-oleate in the reaction medium [82].

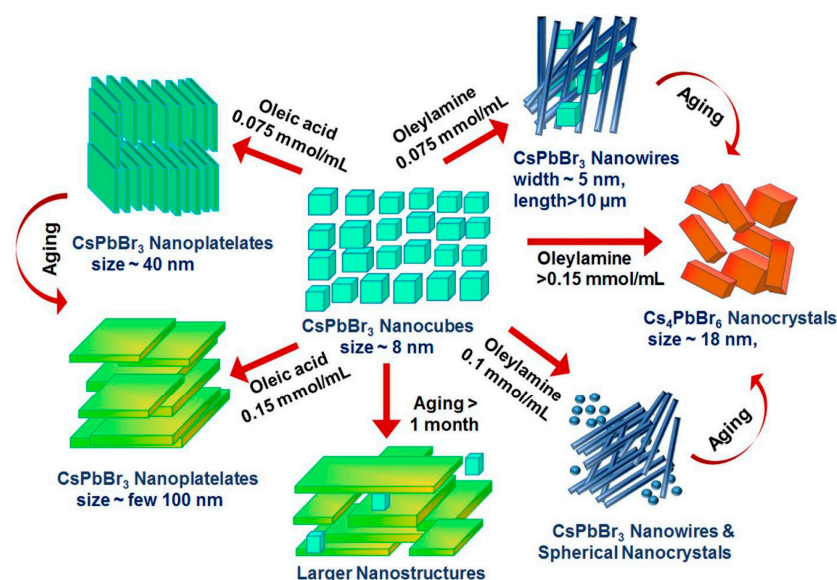


**Figure 5.** Schematic representation of post-synthetic modification of CsPbBr<sub>3</sub> NCs in the presence of OA and OAm. Reprinted with permission from ref. [77] Copyright 2022 American Chemical Society (The results in the image are based on ref. [76]).

The inclusion of excess OA also favors the improvement of PL properties, because the addition of OA reduces the desorption of oleate ions, enhancing the PL characteristics [83]. Despite their equal contribution, it was found that high polar solvents such as acetone selectively remove OAm<sup>+</sup> from the NC surface, leaving OA<sup>-</sup> on it [31]. Thus, weakly bounded OAm<sup>+</sup> ions direct the structure and morphology of Cs LHP NCs. At the same time, OA remains a dense layer on the surface and stimulates the two-dimensional (2D) growth pattern to form NPLs with different thicknesses [17,49]. Here, the OA excess is assumed to exfoliate the structural units, forming different monolayers. Likewise, OA's rich condition in the reaction favors the formation of thicker NPLs, which strongly influence the PL spectra [65]. In addition to this, OA helps to solubilize the cesium source. The solubilization rate depends on the value of heat of formation energy. For example, it is observed that OA and OAm could solubilize cesium acetate (CsCH<sub>3</sub>COO (CsOAc)). In contrast, CsBr and CsCl are only partially solubilized due to the higher heat of the formation energy [4]. In another study, it is evidently observed that replacing Cs<sub>2</sub>CO<sub>3</sub>

with CsOAc is very helpful in achieving Cs LHP NCs with different morphologies in the presence of OA/OAm [31]. The morphological analysis of the formation of CsPbX<sub>3</sub> NWs under the influence of different amounts of HX (X = Cl, Br, I) in the presence of OA/OAm and a comparison graph of the influence of the ratio of OA/OAm on the PL spectra of the CsPbBr<sub>3</sub> NPLs are given in Figure 6.

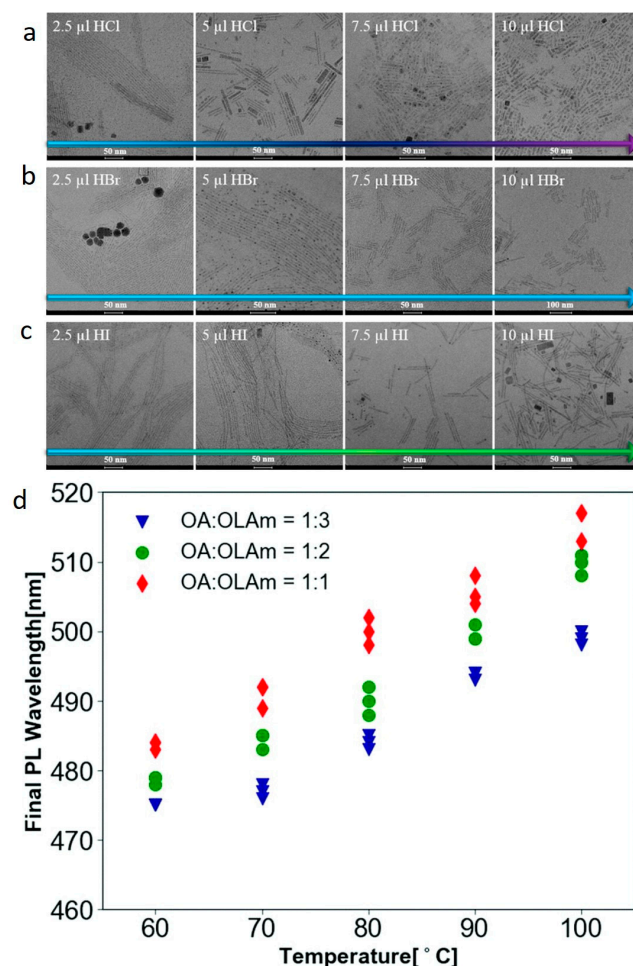


**Figure 6.** (a–c) Formation of CsPbX<sub>3</sub> nanowires in the presence of OA/OAm with increasing amounts of HCl, HBr and HI. Reprinted with permission from ref. [63] Copyright 2017 American Chemical Society, and (d) Correlation of PL wavelength with respect to the reaction temperature under different concentrations of OA/OAm. Reprinted with permission from ref. [65]. Copyright© Royal Society of Chemistry.

Another intriguing aspect of the OA/OAm ligand pair is its capacity for the self-assembly of LHP NCs. The use of OAm and OA direct self-assembled super-lattice structures in NC films due to the solvent, ligand, and light-induced interaction. Self-assembly has been carried out in the nanocubes [44,84], NPLs [85–87], NWs [88,89], and nanorods (NRs) [90] of Cs LHP NCs. Generally, the self-assembly of Cs LHP NCs in solution takes place when the dispersed NCs are kept for a long time. Here, together with OA/OAm, the dielectric constant and polarity of the dispersing solvent significantly influence the rate of the self-assembly process. In the case of NC films, with respect to the solvent and ligands, the self-assembly is influenced. Moreover, surface treatment using smaller molecules could also motivate self-assembly, owing to the close contact of NCs. For example, when CsPbBr<sub>3</sub> nanocubes are treated by thiocyanate (SCN<sup>-</sup>) molecules, the oleyl molecules are partially replaced by SCN<sup>-</sup>, which brings the nanocubes very close to each other, favoring the self-assembly [91]. The interparticle spacing between the OA/OAm-capped NCs in such a supramolecular assembly is approximately 11.4 ± 0.1 nm in the colloidal state [92]. Liu et al.

used a solar simulator with the power of 1.7 suns ( $170 \text{ mW/cm}^2$ ) to remove OA/OAm ligands from the as-synthesized CsPbBr<sub>3</sub> NCs (PL lifetime~2 ns) [88]. In this case, the removal of OA/OAm accelerated the formation of NWs (PL lifetime~125 ns) through self-assembly. Similarly, by varying the intensity of light (532 nm and 670 nm), Pramanik et al. achieved nanobelts and nanoplatelet morphologies from OA/OAm-capped CsPbI<sub>3</sub> QDs [87]. This kind of UV-light irradiation on the 1-alkynyl acid-capped CsPbBr<sub>3</sub> QDs could induce the formation of self-assembled nanostructures through a catalysis reaction in the presence of a reaction intermediate, CsBr [93]. It is possible to achieve self-assembly in Cs LHP NCs by the sole use of OAm as a ligand [94]. Nevertheless, OA could support the achievement of a long-range ordered NC assembly [95]. It is demonstrated that the high concentration of OAm could lead from NSs to NWs through a dipole–dipole interaction in the presence of OA [68]. Bi et al. have indicated that during the self-assembly process, OA is gradually desorbed and under the influence of OAm, the growth of CsPbI<sub>3</sub> NWs takes place [72]. Thus, the structural participation of OAm<sup>+</sup> ions also influences the morphology of Cs LHP NCs. During synthesis, the self-assembled one-dimensional CsPbBr<sub>3</sub> NWs can be achieved by forming lamellar structures [70,96]. Moreover, the OAm-rich synthesis reaction at 180 °C could direct the formation of self-assembled CsPbBr<sub>3</sub> NWs [97]. In this case, the self-assembly of NWs takes place by connecting [PbBr<sub>6</sub>]<sup>4-</sup> octahedrons under a longer reaction period. Furthermore, it is demonstrated that together with these factors, surface halide vacancies of Cs LHP NCs could promote self-assembly [72,98]. The self-assembly of Cs LHP NCs into NWs could be distinguished through a shift in the PL spectrum depending on the aspect ratio. Interestingly, it was found that while aging CsPbBr<sub>3</sub> NCs under ambient conditions, the top surface of the resultant NC super-lattice is converted to bulk-like particles through a coalescence process [99]. Along with morphology, aging Cs LHP NCs could also induce a phase transformation. By aging the pre-synthesized cubic CsPb(Br<sub>x</sub>I<sub>1-x</sub>)<sub>3</sub> NCs in an equal volume of toluene and chloroform, it is possible to achieve orthorhombic CsPb(Br<sub>x</sub>I<sub>1-x</sub>)<sub>3</sub> NWs [100]. In this case, the spontaneous coalescence of NCs leads to NWs through an oriented attachment process. Other than these results, as discussed previously, the post-synthetic transformation of Cs LHP NCs to NWs is also demonstrated. Factors such as dipole–dipole, hydrophobic and van der Waals interactions of the NC capping agents could lead to super-lattice nanostructures in Cs LHP NCs [28,68]. As mentioned, self-assembly is also directed by solvents with different polarity. If the inter-particle spacing between the NCs is less than twice the OA/OAm ligand length (~4 nm), the solvent could induce self-assembly [101]. Mehetor et al. observed a polarity-dependent self-digestive conversion of CsPbBr<sub>3</sub> quantum wires to quantum rods [90]. In this case, the authors observed a rapid conversion of this morphology change in chloroform (CHCl<sub>3</sub>) but a very slow conversion in hexane. Similarly, Soetan et al. observed a one-dimensional super-lattice nanostructure transformation of CsPbBr<sub>3</sub> NCs when redispersed in toluene (non-polar), whereas two-dimensional short-range nanostructures were observed in polar solvents [101]. A mixed-solvent system for ex: toluene/chloroform was also found to be useful in expediting the self-assembly of CsPb(Br<sub>x</sub>I<sub>1-x</sub>)<sub>3</sub> nanocubes to NWs under aging [99]. Here, along with the partial removal of ligands, the strong dipolar interaction of nanocubes leads to the formation of NWs. Similar to these investigations, there are different studies elucidating the role of solvents and ligands in the self-assembly of Cs LHP NCs [102–106]. Because of polarity, alcohols play an important role in the formation of super-lattice nanostructures of Cs LHP NCs. For instance, synthesizing CsPbBr<sub>3</sub> NCs in the presence of methanol/cesium cholates directs the formation of NRs through oriented attachment [47]. Like methanol, the addition of ethanol into pre-synthesized CsPbX<sub>3</sub> NPLs was found to direct the formation of NWs [17]. It was also found that CsPbBr<sub>3</sub> NPLs could spontaneously transform into nanobelts and nanotiles under prolonged storage [107]. This kind of spontaneous self-assembly is generally directed by NC surface ligands through interparticle interactions [108]. In most of these investigations, the desorption of OA/OAm under different conditions leads to super-lattice nanostructures of Cs LHP NCs. The schematic representations of the formation of the one-dimensional super-lattice assembly

of OA/OAm-capped CsPbBr<sub>3</sub> NCs, the two-dimensional OA-induced long-range assembly of CsPbBr<sub>3</sub> NPLs, and the structural and morphological analysis of CsPbBr<sub>3</sub> NCs and NWs are given in Figure 7.

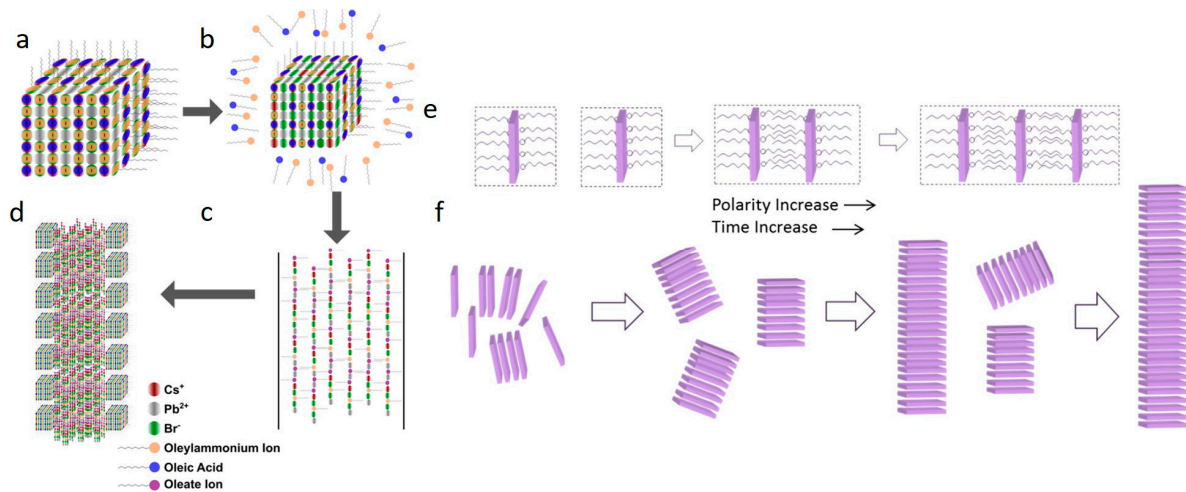


**Figure 7.** (a–d) Schematic representation of formation mechanism of one-dimensional OA/OAm-capped CsPbBr<sub>3</sub> NC super-lattice nanostructures. Reprinted with permission from ref. [101] Copyright 2017 American Chemical Society. (e,f) Schematic representation of formation mechanism of long-range CsPbBr<sub>3</sub> NPLs assembly in the presence of OA. Reprinted with permission from ref. [95] Copyright 2019 American Chemical Society.

### 2.3. Phase Transformation of Cs LHP NCs in the Presence of OA/OAm

A variation in the concentration of OA/OAm will additionally impact the resulting phase of the Cs LHP NCs. Even a slight variation in their concentration alters the structural arrangement of atoms and directs the phase transformation. Two kinds of perovskite phases possibly form under the influence of OA/OAm, namely Cs<sub>4</sub>PbX<sub>6</sub> and CsPb<sub>2</sub>Br<sub>5</sub>. Usually, a high OAm concentration with CsPbBr<sub>3</sub> promotes the formation of the lead-depleted rhombohedral Cs<sub>4</sub>PbBr<sub>6</sub> phase [109–111]. This is actually a reversible transformation that takes place between corner shared PbX<sub>6</sub> octahedra to isolated PbX<sub>6</sub> octahedra. It is observed that the formation of the Cs<sub>4</sub>PbX<sub>6</sub> occurs through forming halo-plumbate species in solution under a high Pb<sup>2+</sup>-ligand ratio [61]. While Cs<sub>4</sub>PbBr<sub>6</sub> itself is non-luminescent, the presence of a small amount of CsPbBr<sub>3</sub> introduces fascinating optical characteristics. This has been experimentally demonstrated by different research groups [112–114]. Jing et al. have adopted an amine-free synthesis approach to synthesize CsPbBr<sub>3</sub> NCs [115]. In this case, the authors have observed that adding OAm with the pre-prepared CsPbBr<sub>3</sub> NCs leads to Cs<sub>4</sub>PbBr<sub>6</sub> phase transformation. This phase transformation by OAm could be accelerated in the presence of potential organic compounds such as thiol [109]. Here, the formation of Cs<sub>4</sub>PbBr<sub>6</sub> NCs is confirmed through the emergence of the peak at ~315 nm in the UV-visible spectra. This phase conversion can be achieved by increasing the concentration of OA/OAm [27]. Furthermore, it is possible to achieve the same when the NCs are redispersed in hexane. The mechanism behind this phase transformation is still unclear. Accordingly, in most of the observations, it is stated that the dissolution-recrystallization accompanied by the influence of excess OAm is the reason for converting the luminescent to the non-luminescent phase [109,116]. Other possibilities, such as ligand environment and soft ligand templating, are also proposed as reasons for this phase transformation. Li et al. observed that when the synthesis reaction is carried out in an OAm-rich atmosphere, temperature and reaction time significantly influence the formation of perovskite NCs [97]. In this case, the authors achieved Cs<sub>4</sub>PbBr<sub>6</sub> NCs at 160 °C and CsPbBr<sub>3</sub> NCs at 180 °C. It was found that in contrast with CsPbBr<sub>3</sub> NCs, where the substitution of Cs<sup>+</sup> takes place by OAm<sup>+</sup> cations, Cs<sub>4</sub>PbBr<sub>6</sub> is comprised of both OAm and OA in a bonded state as an OAm<sup>+</sup>-OA<sup>-</sup> complex [49]. The different roles of OAm and the phase transformation of CsPbBr<sub>3</sub>

NCs under the influence of OA/OAm with their structural, optical, and morphological characterization are combinedly given in Figure 8.

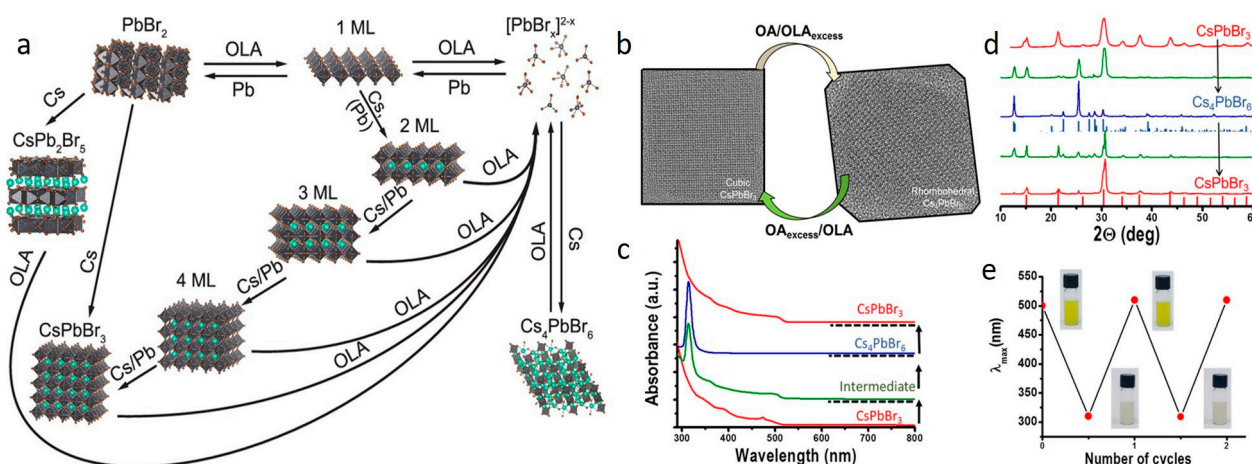


**Figure 8.** (a) Ligand control of the dynamic reversibility between  $\text{CsPbBr}_3$  and  $\text{Cs}_4\text{PbBr}_6$ . Reprinted with permission from ref. [111] Copyright 2020 American Chemical Society. (b) Transmission electron microscopy images of cubic  $\text{CsPbBr}_3$  to  $\text{Cs}_4\text{PbBr}_6$  NCs (from left to right, respectively) using the addition of an excess of OA/OAm. (c) UV-visible spectra of  $\text{CsPbBr}_3$  NCs and  $\text{Cs}_4\text{PbBr}_6$  NCs under the influence of OAm/OA. (d) X-ray diffraction (XRD) of the conversion of  $\text{CsPbBr}_3$  (red) to  $\text{Cs}_4\text{PbBr}_6$  NCs (blue) and back along with the intermediates (green). Bulk XRD spectra for cubic  $\text{CsPbBr}_3$  and  $\text{Cs}_4\text{PbBr}_6$  are given as a bar plot. (e) Two complete  $\text{CsPbBr}_3$ – $\text{Cs}_4\text{PbBr}_6$  NC cycles as followed by UV-visible spectroscopy. Plotted is the wavelength of the first excitonic absorption peak. Reprinted with permission from ref. [110] Copyright 2018 American Chemical Society.

Structural models demonstrate the reversible transformation between luminescent  $\text{CsPbBr}_3$  and non-luminescent  $\text{Cs}_4\text{PbBr}_6$  NCs. In general,  $\text{Cs}_4\text{PbBr}_6$  NCs are obtained after adding an extra number of OA/OAm ligands once the  $\text{CsPbBr}_3$  NCs are synthesized. Reversibly, the  $\text{Cs}_4\text{PbBr}_6$  NCs are transformed back to highly luminescent  $\text{CsPbBr}_3$  NCs after adding  $\text{PbBr}_2$ . The  $\text{CsPbBr}_3$  NCs structure is characterized by corner-sharing  $[\text{PbX}_6]^{4-}$  octahedra with  $\text{Cs}^+$  ions filling the voids created by four neighboring  $[\text{PbX}_6]^{4-}$  octahedra. In the  $\text{Cs}_4\text{PbBr}_6$  NCs structure, adjacent  $[\text{PbBr}_6]^{4-}$  octahedra do not share any corners and they are entirely decoupled in all directions. Thus, excess  $\text{PbBr}_2$  can be integrated into the crystal structure of  $\text{Cs}_4\text{PbBr}_6$  NCs to form compact  $\text{CsPbBr}_3$  NCs [117].

### 3. Potential Ligands and Solvents Replacing OA and OAm: A Step towards Enhancing Optical Properties and Stability of Cs LHP NCs

Although OA and OAm are helpful for the passivation of Cs LHP NCs, their role as ligands is limited. When highly ionic Cs LHP NCs are prepared with OA/OAm ligands, their attachment with the surface is relatively weak, and they could easily detach even during the first purification cycle. This purification step mainly depends on the polarity of the solvents. For instance, solvents such as methyl acetate and ethyl acetate are much preferred compared with acetone, ethanol, and isopropanol. Purification by suitable solvents greatly assists in controlling ligand density in Cs LHP NCs. For example, purification using an ethyl acetate/hexane solvent mixture was found to precisely regulate OA/OAm ligand density in Cs LHP NCs with excellent PL properties [118–120]. When the prepared crude solid Cs LHP NCs undergo multiple purification cycles, the detachment of ligands substantially impacts the colloidal stability as well as the lifetime and PLQY of Cs LHP NCs. The weak binding nature is also attributed to the low binding constant value ( $6020 \text{ M}^{-1}$ ) of  $\text{OAm}^+$  over short-chain amine ions [121]. Moreover, the removal of OA/OAm is also very sensitive to thermal annealing and UV exposure [38].

Recently, this problematic issue has been solved using strong binding ligands. Compared with OA/OAm, these ligands resist the antisolvents and do not detach from the

NC surface during purification. Thus, the colloidal stability and the optical properties are well preserved even after purification, and highly luminescent NCs are achieved. Several kinds of non-traditional ligands and potential additives have been explored recently, and their effect on the NC surface is documented [122,123]. For example, phosphonic ligands are identified as potential candidates that resist solvent washing and produce smaller NCs [124,125]. Here, the P-O bond is relatively stronger, with the  $\text{Pb}^{2+}$  leading to a network with octylphosphonate molecules through hydrogen bonds. Additionally, unlike OA/OAm reversible dynamic binding ligands, the irreversible phosphonate binding results in an increase in PL intensity [57,126]. In addition to binding ability, it is demonstrated that oleylphosphonic acid ( $\text{pK}_a = 2$ ) could effectively replace  $\text{DDA}^+$  ions from the surface of  $\text{CsPbBr}_3$  NCs without affecting the optical properties [127]. Although these ligands provide stability, OAm is still used to dissolve the Pb precursor,  $\text{PbBr}_2$ . However, this use of OAm can be efficiently replaced by TOPO, as demonstrated experimentally [126]. Likewise, a complete amine-free synthesis of  $\text{CsPbBr}_3$  NCs is reported using TOP as a solvent with HBr or 1-bromopropane as a bromide source [128,129].

Interestingly, when trioctylphosphine (TOP) is used as a solvent to synthesize Cs LHP NCs, TOP is oxidized to TOPO and prevents the oxidation of  $\text{Pb}^{2+}$  [130]. Similarly, it is observed that using a quaternary ammonium halide salt, didodecyldimethylammonium bromide (DDAB), instead of OAm significantly improves the PLQY of Cs LHP NCs, up to near-unity [4,127,131]. For this, DDAB in a non-polar solvent, specifically in toluene, is used to carry out the surface modification. Here, DDAB specifically heals the CsX surface vacancies, resulting in an impressive PLQY. Thus, DDAB enables a reduction in the number of ligands present on the surface of Cs LHP NCs without impacting their optical properties. This treatment is particularly useful for improving the charge transport in optoelectronic devices like LEDs [132,133]. Because of the shorter chain length over the OA/OAm ligand pair, DDAB specifically replaces OAm and could efficiently bind on the surface of the Cs LHP NCs [134,135]. The efficiency of DDAB treatment could be enhanced by the inclusion of a co-additive like  $\text{ZnBr}_2$  [134]. However, improving the PLQY using DDAB should be carried out with careful observations, since this may lead to a phase transformation [136,137]. Similar to DDAB, different kinds of organic and inorganic compounds are used for the post-synthetic modification of Cs LHP NCs in solution or in solid-state in order to regulate the density of the OA/OAm binary ligands. Ligand exchange in perovskite NCs is a complex process that requires careful consideration of the desired modifications and their impact on stability and performance. Researchers continue to investigate and refine ligand-exchange techniques to unlock the full potential of perovskite NCs for various applications in optoelectronics and beyond.

During the synthesis reaction, the formation of  $\text{OAmBr}$  frequently leads to a decrease in surface  $\text{Br}^-$  ions on  $\text{CsPbBr}_3$ , leading to a deterioration in optical properties. To prevent this, substituting OAm with HBr is a viable approach. Akhil et al. have adopted this approach and demonstrated the completely amine-free synthesis of  $\text{CsPbBr}_3$  NCs through the hot-injection method [129,138]. Here, it is observed that an increase in  $\text{Br}^-$  concentration results in the formation of  $\text{CsPbBr}_3$  NCs. The authors have observed that excessive halide concentration in the reaction helps to achieve  $\text{CsPbBr}_3$  NCs with high stability. Furthermore, the NC films demonstrated enhanced stability over a three-month period, suggesting the potential of halo acids as a promising alternative to the OA/OAm ligand pair for achieving highly stable and luminescent Cs LHP NCs.

Recently, zwitterionic ligands have been delivering promising results in the stabilization and maintenance of the optical properties of Cs LHP NCs. Zwitterionic ligands are molecules featuring both positively charged groups (e.g., ammonium) and negatively charged groups (e.g., carboxylates, sulfonates, and phosphonates). These bidentate ligands demonstrate a more robust interaction with the surface of NCs and exhibit a lower detachment rate when compared to the OA/OAm ligand pair. Consequently, this allows for the long-term stability of optical properties [139]. In particular, zwitterionic ligands possess strong chelating ability and can stand several purification cycles with different

solvents—for example, ethyl acetate (EtOAc) [140,141]. The existence of acidic and basic functional groups in the same molecule helps to maintain the acid–base equilibria and stabilize the Cs LHP NCs with high durability. An ideal zwitterionic ligand should have a lower diffusion coefficient value and should possess higher binding energy. Moreover, zwitterionic ligands have a different electrokinetic potential value ( $\zeta$ ) to the OA/OAm ligand pair, which derives interesting results in surface passivation [25]. For example, OAm/OA-capped CsPbBr<sub>3</sub> QDs show a  $\zeta$  potential of 9.17 meV, whereas a zwitterionic ligand betaine (BT)-capped QDs show 25.8 meV [142].

Krieg et al. first used different kinds of zwitterionic ligands (sulfobetaine, phosphocholine, soy lecithin and  $\gamma$ -aminoacids) to stabilize orthorhombic CsPbBr<sub>3</sub> NCs [140,143]. It is also possible to synthesize zwitterionic ligands through an in-situ chemical reaction in the presence of OAm [144]. Among these, sulfobetaine is the most used zwitterionic ligand and is characterized by both a quaternary ammonium group (positively charged) and a sulfonate group (negatively charged). The sulfobetaine ligand is quite efficient in passivating Mn<sup>2+</sup>-doped alloyed Cs LHP NCs with a high PLQY and could minimize the reabsorption effect [145]. Lee et al. used a sulfobetaine ligand, 3-(dodecyl-dimethylammonio)-propane-1-sulfonate (12-SBE), to passivate CsPbBr<sub>3</sub> NCs [146]. In this case, the 12-SBE modified NCs showed a near-unity PLQY, long PL lifetime, less agglomeration, and high stability. Although sulfobetaine efficiently binds to the Cs LHP NCs, TOPO is necessary to achieve monodispersed, highly stable CsPbBr<sub>3</sub> NCs [147]. Unfortunately, the sulfobetaine-capped CsPbBr<sub>3</sub> NCs show worse charge transport properties and a lack of electronic coupling compared to the DDAB-capped CsPbBr<sub>3</sub> NCs [139,148,149]. This highlights the need for the molecular engineering of zwitterionic ligands. Various kinds of zwitterionic ligands such as aromatic [141], polymeric [150–152], photo-crosslinkable [153], amino acids [154], modular zwitterion functionalized polymers [155], carbazole [156], and quaternary ammonium halide-based zwitterionic ligands [157] show an important role in stabilizing highly luminescent Cs LHP NCs are explored. Interestingly, Zhu et al. have proposed that both surface-selective and non-selective ligands are necessary to control the morphology and stability of CsPbBr<sub>3</sub> NCs [157]. The authors have demonstrated that zwitterionic ligands are surface-selective to achieve anisotropic nanostructures (nanocubes, NPLs and NRs), and dodecylamine (DDA)-based surface non-selective ligands could assist for it along with stability. In most cases, the OA/OAm ligands of Cs LHP NCs are post-synthetically exchanged by zwitterionic ligands via a partial ligand exchange, and the resultant NC properties are analyzed. Figure 9 provides a schematic overview of the interaction between OA/OAm and zwitterionic ligands with the perovskite NC surface. It also highlights the properties of zwitterionic ligands in solution and in the solid state. Additionally, the figure offers a collective representation of the chemical structure, synthesis process, and key findings related to the PLQY and the ligand-exchange ratio for 12-SBE-capped CsPbBr<sub>3</sub> NCs.

Similar to zwitterionic ligands, multidentate ligands are also helpful in stabilizing Cs LHP NCs with improved robustness. Multidentate ligands strongly coordinate with the Cs LHP NC surface, forming a shell to protect the moisture-sensitive Cs LHP NCs. For example, a silane-based branched ligand such as n-propyltrimethoxysilane-dimethyloctadecylammonium bromide (PDB) was found to polymerize on the surface of the CsPbBr<sub>3</sub> QDs and impart high stability [158]. Similarly, 3-mercaptopropyltrimethoxysilane (MPTMS) in 1-octanethiol could induce a hybrid polymerization for the stabilization of CsPbBr<sub>3</sub> NCs [159]. Also, growing CsPbBr<sub>3</sub> NCs in the micelles of a polymeric multidentate ligand, polystyrene-*block*-poly-2-vinyl pyridine (PS-*b*-P2VP), was found to be useful in reducing the polar solvent diffusion into the Cs LHP NCs [160]. Multidentate ligands such as ethylenediamine tetraacetic acid (EDTA) [161,162], trithiocarbonate terminated polymeric ligand [163], poly-ethylene glycol (PEG)-based polymeric molecule [151,164], polyethyleneimine [165], quaternary ammonium- or imidazolium-based polysalt ligand [166,167], picolinate [168], sulphur-tributylphosphine (S-TBP) bidentate ligand [169], tetramethylthiuram disulfide (TMTD) [170], etc., have proven their strong binding ability with the surface of Cs LHP NCs. Zeng et al. used

bis(2,4,4-trimethylpentyl) phosphonic acid to protonate a multidentate amine ligand, *N'*-(2-aminoethyl)-*N'*-hexadecylethane-1,2-diamine (AHDA) [171]. These protonated AHDA-capped CsPbI<sub>3</sub> NCs showed lower diffusion coefficient ( $66 \pm 3.4 \mu\text{m}^2 \text{s}^{-1}$ ) and higher binding energy value (2.36 eV) over traditional OAM-capped NCs. This shows that novel ligands with a higher binding energy value could be resistant to traditional washing solvents of Cs LHP NCs and retain long-term optical properties. From the application point of view, the surface-modified Cs LHP NCs using zwitterionic and multidentate ligands are beneficial for photocatalysis applications, as evidenced by their high stereoselectivity in C-C oxidative coupling reactions [152,172] and also in the fabrication of light-emitting diodes (LEDs) [146,165,170].

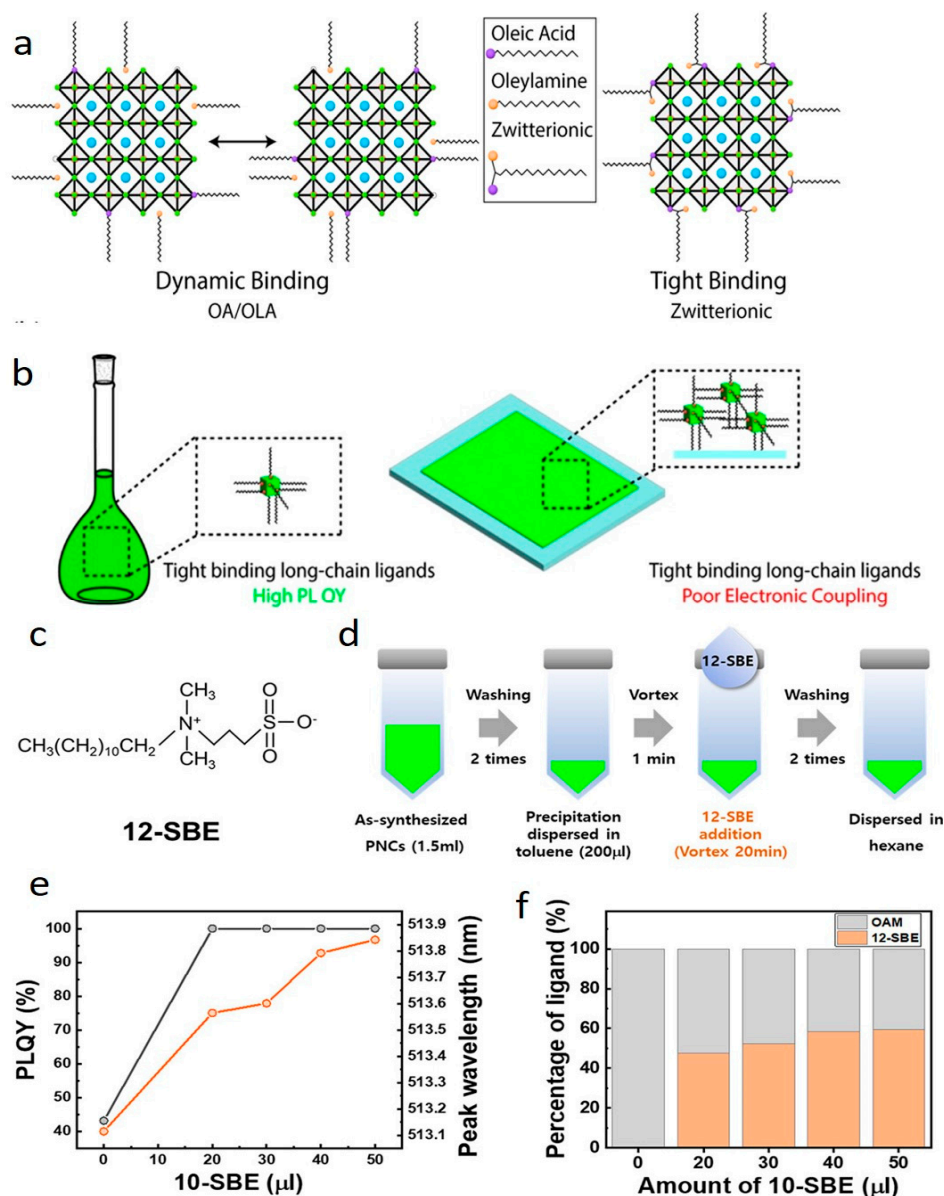


**Figure 9.** (a) Schematic representation of dynamic binding (OA/OAm binary ligands capping) and tight binding (zwitterionic ligand capping) of Cs LHP NCs. (b) Schematic representation of properties of tight binding long-chain ligands in solution and in solid state. Reprinted with permission from ref. [139] Copyright 2022 American Chemical Society. (c,d) Chemical structure and scheme of synthesis and redispersion of 12-SBE-capped CsPbBr<sub>3</sub> NCs. (e,f) Comparative plots of PLQY and ratio of ligand exchange with different volume additions of 12-SBE zwitterionic ligand. Reprinted with permission from ref. [146] Copyright 2023 American Chemical Society.

Other than these systems, several kinds of post-treatment approaches using a wide variety of compounds have been demonstrated to strip the native OA/OAm ligand pair and/or to passivate the surface defects of Cs LHP NCs [11,46,173]. These surface treatment processes impressively enhance the PLQY of Cs LHP NCs. All these findings clearly indicate the emergence of potential, alternative anchoring ligands for designing surface-tailored Cs LHP NCs by replacing the OA/OAm ligand pair. Figure 10 presents three key aspects: the surface ligand content of AHDA<sup>-</sup> and OA/OAm-capped CsPbI<sub>3</sub> NCs with respect to purification cycles; a schematic illustration depicting the interaction of capping ligands with the surface of perovskite NCs; and diffusion coefficient values for OA/OAm- and AHDA-capped CsPbI<sub>3</sub> NCs. Additionally, it shows the chemical structure and a schematic representation of picolinate capping on the surface of perovskite NCs.

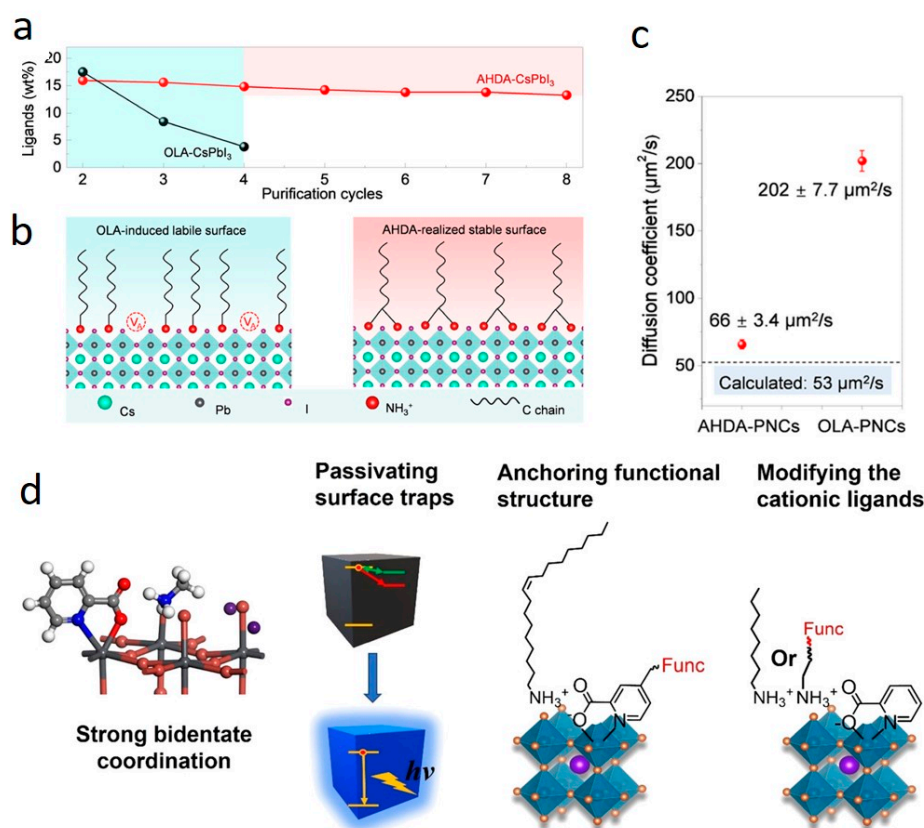


**Figure 10.** (a) Comparison graph of surface ligand content of AHDA- and OA/OAm-capped CsPbI<sub>3</sub> NCs with respect to purification cycles. (b) Schematic representation of AHDA and OA/OAm stabilization of CsPbI<sub>3</sub> NCs. V<sub>A</sub> represents a ligand vacancy. (c) Diffusion coefficient values of OA/OAm- and AHDA-capped CsPbI<sub>3</sub> NCs, determined by diffusion-ordered spectroscopy (DOSY). Reprinted with permission from ref. [172] Copyright 2022 American Chemical Society. (d) Crystal structure of strongly bound picolinate ligand and schematic representation of its passivation on the perovskite NC surface. Reprinted with permission from ref. [169] Copyright 2021 American Chemical Society.

In general, improving the photostability and thermal stability of perovskite NCs is indeed a crucial area of research and development. However, their stability issues have been a significant challenge that needs to be addressed for widespread commercialization. Apart from the use of ligands, there are some strategies and recommendations to enhance the stability of Cs LHP NCs:

- (i) Encapsulation and passivation: One of the primary reasons for perovskite instability is exposure to moisture, oxygen, and light. Encapsulation techniques involving pro-

protective coatings or capping ligands can shield Cs LHP NCs from these environmental factors. The passivation of surface defects can also improve stability [22].

- (ii) **Composition engineering:** Modifying the chemical composition of Cs LHP NCs by incorporating elements with higher stability, such as lead-free perovskites or mixed-halide perovskites, can enhance their resistance to degradation.
- (iii) **Structural modifications:** Researchers have explored alternative perovskite structures, such as double perovskites and 2D perovskites, which may exhibit improved stability compared to traditional 3D perovskites.
- (iv) **Doping:** Introducing suitable dopants into Cs LHP NCs can improve their stability and performance. For example, incorporating small amounts of certain metal ions can passivate defects and reduce degradation.
- (v) **Stabilizing additives:** The use of stabilizing additives or polymer matrices in perovskite NC films can improve their resistance to environmental factors and enhance long-term stability [174].

Overall, addressing the stability challenges of perovskite NCs is a critical step toward unlocking their full potential for various applications. Research and development efforts focused on stability enhancement will play a pivotal role in the successful commercialization of perovskite-based technologies.

#### 4. Conclusions and Summary

This discussion narrates the crucial role of OA/OAm in synthesizing Cs LHP NCs. These binary ligands help to fabricate highly crystalline, highly ordered nanostructures and films of Cs LHP NCs. All the existing analyses show that it is essential to understand the reaction chemistry to explore other possible roles of these binary ligands. It is possible to obtain all kinds of phases and morphologies of Cs LHP NCs by cleverly tuning the concentration and ratio of the OA/OAm in the reaction. The experimental findings also reveal the critical role of OAm in the structural framework of perovskite NCs, a decisive factor in achieving highly luminescent characteristics. Although OA/OAm plays an essential role in the synthesis, a clear understanding should be established to invest the knowledge of this into other types of perovskite NCs. Also, the active role of these binary ligands is not much studied for lead-free perovskite NCs and requires timely exploration.

Furthermore, multidentate ligands that could couple with OA and OAm to contribute strong binding ability should be developed. Also, promising ligands that help to avoid morphology and phase transformation in the presence of OA/OAm are helpful for long-term applications. In this view, zwitterionic ligands can be considered to develop Cs LHP NCs with excellent stability and superior optical properties. Replacing OA and OAm with alternative bidentate ligands is a relatively reasonable effort in stabilizing highly luminescent perovskite NCs. Moreover, it is essential to analyze the spectroscopic characteristics of NCs synthesized using OA- and OAm-free solvents to understand the nature of bonding. Still, the role of OA and OAm impart better control of the morphology and phase, as seen in this discussion. Future accomplishments in this view would reveal many interesting findings in determining the structure and phase of perovskite NCs, which is helpful for several promising applications.

**Author Contributions:** Conceptualization, A.S. (Ananthakumar Soosaimanickam) and R.A.; validation, A.S. (Alejandro Saura) and N.F. (Noemi Farinos); writing—original draft preparation, A.S. (Ananthakumar Soosaimanickam), A.S. (Alejandro Saura) and N.F.; writing—review and editing, A.S. (Ananthakumar Soosaimanickam), N.F. and R.A.; visualization, A.S. (Alejandro Saura) and R.A.; project administration, R.A.; funding acquisition, R.A. All authors have read and agreed to the published version of the manuscript.

**Funding:** The authors would like to acknowledge the funding by MCIN/AEI/10.13039/501100011033 (Research projects no. PID2020-119628RB-C31, PID2020-119628RB-C32 and PID2019-104272RB-C53). This study forms part of the Advanced Materials Programme and was supported by MCIN with funding from the European Union Next Generation EU (PRTR-C17.I1) and by the Generalitat Valen-

ciana (codes MFA/2022/040 and MFA/2022/007). The work was partially funded by MCIN/AEI through project TED2021-131600B-C32.

**Conflicts of Interest:** The authors declare no conflict of interest.

## References

1. Pan, Y.; Zhang, Y.; Kang, W.; Deng, N.; Yan, Z.; Sun, W.; Kang, X.; Ni, J. Progress in the preparation and application of CsPbX<sub>3</sub> perovskites. *Mater. Adv.* **2022**, *3*, 4053–4068. [[CrossRef](#)]
2. Aznar-Gadea, E.; Sanchez-Alarcon, I.; Soosaimanickam, A.; Rodriguez-Canto, P.J.; Perez-Pla, F.; Martinez-Pastor, J.P.; Abargues, R. Molecularly imprinted nanocomposites of CsPbBr<sub>3</sub> nanocrystals: An approach towards fast and selective gas sensing of explosive taggants. *J. Mater. Chem. C* **2022**, *10*, 1754–1766. [[CrossRef](#)]
3. Dong, H.; Ran, C.; Gao, W.; Li, M.; Xia, Y.; Huang, W. Metal halide perovskite for next-generation optoelectronics: Progresses and prospects. *eLight* **2023**, *3*, 3. [[CrossRef](#)]
4. De Trizio, L.; Infante, I.; Manna, L. Surface chemistry of lead halide perovskite colloidal nanocrystals. *Acc. Chem. Res.* **2023**, *56*, 1815–1825. [[CrossRef](#)]
5. Kirakosyan, A.; Kim, Y.; Sihn, M.R.; Jeon, M.-G.; Jeong, J.-R.; Choi, J. Solubility-controlled room-temperature synthesis of cesium lead halide perovskite nanocrystals. *ChemNanoMat* **2020**, *6*, 1863–1869. [[CrossRef](#)]
6. Navarro-Arenas, J.; Suarez, K.; Chirvony, V.S.; Gualdron-Reyes, A.F.; Mora-Sero, I.; Martinez-Pastor, J. Single-exciton amplified spontaneous emission in thin films of CsPbX<sub>3</sub> (X = Br, I) perovskite nanocrystals. *J. Phys. Chem. Lett.* **2019**, *10*, 6389–6398. [[CrossRef](#)]
7. Chen, Y.; Li, F.; Zhang, M.; Yang, Z. Recent progress on boosting the perovskite film quality of all-inorganic perovskite solar cells. *Coatings* **2023**, *13*, 281. [[CrossRef](#)]
8. Ekanayaka, T.K.; Richmond, D.; McCormick, M.; Nandyala, S.R.; Helfrich, H.C.; Sinitskii, A.; Pikal, J.M.; Ilie, C.C.; Dowben, P.A.; Yost, A.J. Surface versus bulk state transitions in inkjet-printed all-inorganic perovskite quantum dot films. *Nanomaterials* **2022**, *12*, 3956. [[CrossRef](#)]
9. Dutta, A.; Behera, R.K.; Pal, P.; Baitalik, S.; Pradhan, N. Near-unity photoluminescence quantum efficiency for all CsPbX<sub>3</sub> (X = Cl, Br and I) perovskite nanocrystals: A generic synthesis approach. *Angew. Chem.* **2019**, *58*, 5552–5556. [[CrossRef](#)]
10. Yang, D.; Li, X.; Wu, Y.; Wei, C.; Qin, Z.; Zhang, C.; Sun, Z.; Li, Y.; Wang, Y.; Zeng, H. Surface halogen compensation for robust performance enhancements of CsPbX<sub>3</sub> perovskite quantum dots. *Adv. Mater.* **2019**, *7*, 1900276. [[CrossRef](#)]
11. Gualdron-Reyes, A.; Masi, S.; Mora-Sero, I. Progress in halide-perovskite nanocrystals with near-unity photoluminescence quantum yield. *Trends Chem.* **2021**, *3*, 499–511. [[CrossRef](#)]
12. Ibaceta-Jana, J.; Muydinov, R.; Rosado, P.; Mirhosseini, H.; Chug, M.; Nazarenko, O.; Dirin, D.N.; Heinrich, D.; Wagner, M.R.; Kuhne, T.D.; et al. Vibrational dynamics in lead halide hybrid perovskites investigated by Raman spectroscopy. *Phys. Chem. Chem. Phys.* **2020**, *22*, 5604–5614. [[CrossRef](#)]
13. Jeong, D.-N.; Yang, J.-M.; Park, N.-G. Roadmap on halide perovskite and related devices. *Nanotechnology* **2020**, *31*, 152001. [[CrossRef](#)] [[PubMed](#)]
14. Huang, Y.; Cohen, T.A.; Sperry, B.M.; Larson, H.; Nguyen, H.A.; Homer, M.K.; Dou, F.Y.; Jacoby, L.M.; Cossairt, B.M.; Gamelin, D.R.; et al. Organic building blocks at inorganic nanomaterial interfaces. *Mater. Horiz.* **2022**, *9*, 61–87. [[CrossRef](#)]
15. Wang, X.; Liu, Y.; Liu, N.; Sun, R.; Zheng, W.; Liu, H.; Zhang, Y. Revisiting the nanocrystal formation process of zero-dimensional perovskite. *J. Mater. Chem. A* **2021**, *9*, 4658–4663. [[CrossRef](#)]
16. Huang, H.; Feil, M.W.; Fuchs, S.; Debnath, T.; Richter, A.F.; Tong, Y.; Wu, L.; Wang, Y.; Dobliger, M.; Nickel, B. Growth of perovskite CsPbBr<sub>3</sub> nanocrystals and their formed superstructures revealed by in situ spectroscopy. *Chem. Mater.* **2020**, *32*, 8877–8884. [[CrossRef](#)]
17. Udayabhaskararao, T.; Kazes, M.; Houben, L.; Lin, H.; Oron, D. Nucleation, growth and structural transformations of perovskite nanocrystals. *Chem. Mater.* **2017**, *29*, 1302–1308. [[CrossRef](#)]
18. Bodnarchuk, M.I.; Boehme, S.C.; ten Brinck, S.; Bernasconi, C.; Shynkarenko, Y.; Krieg, F.; Widmer, R.; Aeschlimann, B.; Gunther, D.; Kovalenko, M.V.; et al. Rationalizing and controlling the surface structure and electronic passivation of cesium lead halide nanocrystals. *ACS Energy Lett.* **2019**, *4*, 63–74. [[CrossRef](#)]
19. Wei, S.; Yang, Y.; Kang, X.; Wang, L.; Huang, L.; Pan, D. Room temperature and gram-scale synthesis of CsPbX<sub>3</sub> (X = Cl, Br, I) perovskite nanocrystals with 50–58% photoluminescence quantum yields. *Chem. Commun.* **2016**, *52*, 7265–7268. [[CrossRef](#)]
20. Yu, W.; Wei, M.; Tang, Z.; Zou, H.; Li, L.; Zou, Y.; Yang, S.; Wang, Y.; Zhang, Y.; Li, X.; et al. Separating crystal growth from nucleation enables the in situ controllable synthesis of nanocrystals for efficient perovskite light-emitting diodes. *Adv. Mater.* **2023**, *35*, 2301114. [[CrossRef](#)]
21. Abargues, R.; Navarro, J.; Rodriguez-Canto, P.; Maulu, A.; Sanchez-Royo, J.F.; Martinez-Pastor, J.P. Enhancing the photocatalytic properties of PbS QD solids: The ligand exchange approach. *Nanoscale* **2019**, *11*, 1978–1987. [[CrossRef](#)] [[PubMed](#)]
22. Soosaimanickam, A.; Adl, H.P.; Chirvony, V.; Rodriguez-Canto, P.J.; Martinez-Pastor, J.P.; Abargues, R. Effect of alkali metal nitrate treatment on the optical properties of CsPbBr<sub>3</sub> nanocrystal films. *Mater. Lett.* **2021**, *305*, 130835. [[CrossRef](#)]

23. Arenas, J.N.; Soosaimanickam, A.; Adl, H.P.; Abargues, R.; Boix, P.P.; Rodriguez-Canto, P.J.; Martinez-Pastor, J.P. Ligand-length modification in CsPbBr<sub>3</sub> perovskite nanocrystals and bilayers with PbS quantum dots for improved photodetection performance. *Nanomaterials* **2020**, *10*, 1297. [[CrossRef](#)] [[PubMed](#)]
24. Adhikari, G.C.; Thapa, S.; Yue, Y.; Zhu, H.; Zhu, P. Near unity PLQY and high stability of barium thiocyanate based all-inorganic perovskites and their applications in white light-emitting diodes. *Photonics* **2021**, *8*, 209. [[CrossRef](#)]
25. Dong, Y.; Wang, Y.-K.; Yuan, F.; Johnston, A.; Liu, Y.; Ma, D.; Choi, M.-J.; Chen, B.; Chekini, M.; Baek, S.-W.; et al. Bipolar-shell resurfacing for blue LEDs based on strongly confined perovskite quantum dots. *Nat. Nanotechnol.* **2020**, *15*, 668–674. [[CrossRef](#)]
26. Akkerman, Q.A.; Park, S.; Radicchi, E.; Nunzi, F.; Mosconi, E.; De Angelis, F.; Brescia, R.; Rastogi, P.; Prato, M.; Manna, L. Nearly monodisperse insulator Cs<sub>4</sub>PbX<sub>6</sub> (X = Cl, Br, I) nanocrystals, their mixed halide compositions, and their transformation into CsPbX<sub>3</sub> nanocrystals. *Nano Lett.* **2017**, *17*, 1924–1930. [[CrossRef](#)]
27. Almeida, G.; Goldoni, L.; Akkerman, Q.; Dang, Z.; Khan, A.H.; Marras, S.; Moreels, I.; Manna, L. Role of acid-base equilibria in the size, shape and phase control of cesium lead bromide nanocrystals. *ACS Nano* **2018**, *12*, 1704–1711. [[CrossRef](#)]
28. Jana, A.; Meena, A.; Patil, S.A.; Jo, Y.; Cho, S.; Park, Y.; Sree, V.G.; Kim, H.; Im, H.; Taylor, R.A. Self-assembly of perovskite nanocrystals. *Prog. Mater. Sci.* **2022**, *129*, 100975. [[CrossRef](#)]
29. Sanchez-Alarcon, R.I.; Noguera-Gomez, J.; Chirvony, V.S.; Pashei Adl, H.; Boix, P.P.; Alarcon-Flores, G.; Martinez-Pastor, J.P.; Abargues, R. Spray-driven halide exchange in solid-state CsPbX<sub>3</sub> nanocrystal films. *Nanoscale* **2022**, *14*, 13214–13226. [[CrossRef](#)]
30. De Roo, J.; Ibanez, M.; Geiregat, P.; Nedelcu, G.; Walravens, W.; Maes, J.; Martins, J.C.; Driessche, I.V.; Kovalenko, M.V.; Hens, Z. Highly dynamic ligand binding and light absorption coefficient of cesium lead bromide perovskite nanocrystals. *ACS Nano* **2016**, *10*, 2071–2081. [[CrossRef](#)]
31. Pan, A.; He, B.; Fan, X.; Liu, Z.; Urban, J.J.; Alivisatos, A.P.; He, L.; Liu, Y. Insight into the ligand-mediated synthesis of colloidal CsPbBr<sub>3</sub> perovskite nanocrystals: The role of organic acid, base, and cesium precursors. *ACS Nano* **2016**, *10*, 7943–7954. [[CrossRef](#)] [[PubMed](#)]
32. Maulu, A.; Navarro-Arenas, J.; Rodriguez-Canto, P.J.; Sanchez-Royo, J.F.; Abargues, R.; Suarez, I.; Martinez-Pastor, J.P. Charge transport in trap-sensitized infrared PbS quantum-dot-based photoconductors: Pros and cons. *Nanomaterials* **2018**, *8*, 677. [[CrossRef](#)] [[PubMed](#)]
33. Maulu, A.; Rodriguez-Canto, P.J.; Navarro-Arenas, J.; Abargues, R.; Sanchez-Royo, J.F.; Garcia-Calzada, R.; Martinez-Pastor, J.P. Strongly-coupled PbS QD solids by doctor blading for IR photodetection. *RSC Adv.* **2016**, *6*, 80201–80212. [[CrossRef](#)]
34. Protesescu, L.; Yakunin, S.; Bodnarchuk, M.I.; Krieg, F.; Caputo, R.; Hendon, C.H.; Yang, R.X.; Walsh, A.; Kovalenko, M.V. Nanocrystals of cesium lead halide perovskites (CsPbX<sub>3</sub>, X = Cl, Br, and I): Novel optoelectronic materials showing bright emission with wide color gamut. *Nano Lett.* **2015**, *15*, 3692–3696. [[CrossRef](#)]
35. Shen, Z.; Zhao, S.; Song, D.; Xu, Z.; Qiao, B.; Song, P.; Bai, Q.; Cao, J.; Zhang, G.; Swelm, W. Improving the quality and luminescence performance of all-inorganic perovskite nanomaterials for light-emitting devices by surface engineering. *Small* **2020**, *16*, 1907089. [[CrossRef](#)]
36. Toso, S.; Baranov, D.; Manna, L. Metamorphoses of cesium lead halide nanocrystals. *Acc. Chem. Res.* **2021**, *54*, 498–508. [[CrossRef](#)]
37. Kumawat, N.K.; Liu, X.-K.; Kabra, D.; Gao, F. Blue perovskite light-emitting diodes: Progress, challenges and future directions. *Nanoscale* **2019**, *11*, 2109–2120. [[CrossRef](#)]
38. Moyon, E.; Kanwat, A.; Cho, S.; Jun, H.; Aad, R.; Jang, J. Ligand removal and photo-activation of CsPbBr<sub>3</sub> quantum dots for enhanced optoelectronic devices. *Nanoscale* **2018**, *10*, 8591–8599. [[CrossRef](#)]
39. Zhang, Q.; Diao, F.; Xue, X.; Sheng, X.; Barba, D.; Wang, Y. Self-assembly of CsPbBr<sub>3</sub> nanocubes into 2D nanosheets. *ACS Appl. Mater. Interfaces* **2021**, *13*, 44777–44785. [[CrossRef](#)]
40. Huang, H.; Raith, J.; Kershaw, S.V.; Kalytchuk, S.; Tomanec, O.; Jing, L.; Susha, A.S.; Rogach, A.L. Growth mechanism of strongly emitting CH<sub>3</sub>NH<sub>3</sub>PbBr<sub>3</sub> perovskite nanocrystals with a tunable bandgap. *Nat. Comm.* **2017**, *8*, 996. [[CrossRef](#)]
41. Yin, J.; Yang, H.; Gutierrez-Arzaluz, L.; Zhou, Y.; Bredas, J.-L.; Bakr, O.M.; Mohammed, O.F. Luminescence and stability enhancement of inorganic perovskite nanocrystals via selective surface ligand binding. *ACS Nano* **2021**, *15*, 17998–18005. [[CrossRef](#)] [[PubMed](#)]
42. Protesescu, L.; Yakunin, S.; Nazarenko, O.; Dirin, D.N.; Kovalenko, M.V. Low-cost synthesis of highly luminescent colloidal lead halide perovskite nanocrystals by wet ball milling. *ACS Appl. Nano Mater.* **2018**, *1*, 1300–1308. [[CrossRef](#)] [[PubMed](#)]
43. Seth, S.; Samanta, A. A facile methodology for engineering the morphology of CsPbX<sub>3</sub> perovskite nanocrystals under ambient condition. *Sci. Rep.* **2016**, *6*, 37693. [[CrossRef](#)]
44. Yuan, Y.; Liu, Z.; Liu, Z.; Peng, L.; Li, Y.; Tang, A. Photoluminescence and self-assembly of cesium lead halide perovskite nanocrystals: Effects of chain length of organic amines and reaction temperature. *Appl. Surf. Sci.* **2017**, *405*, 280–288. [[CrossRef](#)]
45. Stoffel, J.T.; Tsui, E.Y. Stability effects of selective anion abstraction from cesium lead halide perovskite nanocrystals. *J. Phys. Chem. C* **2023**, *127*, 2285–2293. [[CrossRef](#)]
46. Dutt, V.G.V.; Akhil, S.; Mishra, N. Surface passivation strategies for improving photoluminescence and stability of cesium lead halide perovskite nanocrystals. *ChemNanoMat* **2020**, *6*, 1730–1742. [[CrossRef](#)]
47. Chakrabarty, A.; Satija, S.; Gangwar, U.; Sapra, S. Precursor-mediated synthesis of shape-controlled colloidal CsPbBr<sub>3</sub> perovskite nanocrystals and their nanofiber directed self-assembly. *Chem. Mater.* **2020**, *32*, 721–733. [[CrossRef](#)]
48. Pradhan, N. Alkylammonium halides for facet reconstruction and shape modulation in lead halide perovskite nanocrystals. *Acc. Chem. Res.* **2021**, *54*, 1200–1208. [[CrossRef](#)]

49. Kazes, M.; Udayabhaskararao, T.; Dey, S.; Oron, D. Effect of surface ligands in perovskite nanocrystals: Extending in and reaching out. *Acc. Chem. Res.* **2021**, *54*, 1409–1418. [[CrossRef](#)]
50. Kirakosyan, A.; Chinh, N.D.; Sihm, M.R.; Jeon, M.-G.; Jeong, J.-R.; Kim, D.; Jang, J.H.; Choi, J. Mechanistic insight into surface defect control in perovskite nanocrystals: Ligands terminate the valence transition from  $\text{Pb}^{2+}$  to metallic  $\text{Pb}^0$ . *J. Phys. Chem. Lett.* **2019**, *10*, 4222–4228. [[CrossRef](#)]
51. Chen, T.; Xu, Y.; Xie, Z.; Jiang, W.; Wang, L.; Jiang, W. Ionic liquid assisted preparation and modulation of the photoluminescence kinetics for highly efficient  $\text{CsPbX}_3$  nanocrystals with improved stability. *Nanoscale* **2020**, *12*, 9569–9580. [[CrossRef](#)] [[PubMed](#)]
52. Sun, W.; Yun, R.; Liu, Y.; Zhang, X.; Yuan, M.; Zhang, L.; Li, X. Ligands in lead halide perovskite nanocrystals: From synthesis to optoelectronic applications. *Small* **2023**, *19*, 2205950. [[CrossRef](#)]
53. Yassitepe, E.; Yang, Z.; Voznyy, O.; Kim, Y.; Walters, G.; Castaneda, J.A.; Kanjanaboos, P.; Yuan, M.; Gong, X.; Fan, F.; et al. Amine-free synthesis of cesium lead halide perovskite quantum dots for efficient light-emitting diodes. *Adv. Funct. Mater.* **2016**, *26*, 8757–8763. [[CrossRef](#)]
54. Smock, S.R.; Chen, Y.; Rossini, A.J.; Brutchey, R.L. The surface chemistry and structure of colloidal lead halide perovskite nanocrystals. *Acc. Chem. Res.* **2021**, *54*, 707–718. [[CrossRef](#)] [[PubMed](#)]
55. Ravi, V.K.; Santra, P.K.; Joshi, N.; Chugh, J.; Singh, S.K.; Rensmo, H.; Ghosh, P.; Nag, A. Origin of the substitution mechanism for the binding of organic ligands on the surface of  $\text{CsPbBr}_3$  perovskite nanocubes. *J. Phys. Chem. Lett.* **2017**, *8*, 4988–4994. [[CrossRef](#)]
56. Bertolotti, F.; Nedelcu, G.; Vivani, A.; Cervellino, A.; Masciocchi, N.; Guagliardi, A.; Kovalenko, M.V. Crystal structure, morphology and surface termination of cyan-emissive, six-monolayers-thick  $\text{CsPbBr}_3$  nanoplatelets from X-ray total scattering. *ACS Nano* **2019**, *13*, 14294–14307. [[CrossRef](#)]
57. Chen, Y.; Smock, S.R.; Flintgruber, A.H.; Perras, F.A.; Brutchey, R.L.; Rossini, A.J. Surface termination of  $\text{CsPbBr}_3$  perovskite quantum dots determined by solid-state NMR spectroscopy. *J. Am. Chem. Soc.* **2020**, *142*, 6117–6127. [[CrossRef](#)]
58. Ng, C.K.; Wang, C.; Jasieniak, J.J. Synthetic evolution of colloidal metal halide perovskite nanocrystals. *Langmuir* **2019**, *35*, 11609–11628. [[CrossRef](#)]
59. Park, J.; Park, S.; Cho, S.; Kim, Y.; Kim, H.; Jeong, S.; Woo, J.Y. Air-stable cesium lead bromide perovskite nanocrystals via post-synthetic treatment with oleylammonium bromides. *New J. Chem.* **2022**, *46*, 19514–19522. [[CrossRef](#)]
60. Grisorio, R.; Di Clemente, M.E.; Fanizza, E.; Allegretta, I.; Altamura, D.; Striccoli, M.; Terzano, R.; Giannini, C.; Irimia-Vladu, M.; Suranna, G.P. Exploring the surface chemistry of cesium lead halide perovskite nanocrystals. *Nanoscale* **2019**, *11*, 986–999. [[CrossRef](#)]
61. Qu, R.; Zou, L.; Qi, X.; Liu, C.; Zhao, W.; Yan, J.; Zhang, Z.; Wu, Y. Changing the shape and optical properties of  $\text{CsPbBr}_3$  perovskite nanocrystals with hydrohalic acids using a room-temperature synthesis process. *CrystEngComm* **2022**, *22*, 1853–1857. [[CrossRef](#)]
62. Mourdikoudis, S.; Menelaou, M.; Fiuza-Maneiro, N.; Zheng, G.; Wei, S.; Perez-Juste, J.; Polavarapu, L.; Sofer, Z. Oleic acid/oleylamine ligand pair: A versatile combination in the synthesis of colloidal nanoparticles. *Nanoscale Horiz.* **2022**, *7*, 941–1015. [[CrossRef](#)]
63. Amgar, D.; Stern, A.; Rotem, D.; Porath, D.; Etgar, L. Tunable length and optical properties of  $\text{CsPbX}_3$  ( $X = \text{Cl}, \text{Br}, \text{I}$ ) nanowires with a few unit cells. *Nano Lett.* **2017**, *17*, 1007–1013. [[CrossRef](#)] [[PubMed](#)]
64. Akkerman, Q.A.; Motti, S.G.; Kandada, A.R.S.; Mosconi, E.; D’Innocenzo, V.; Bertoni, G.; Marras, S.; Kamino, B.A.; Miranda, L.; De Angelis, F.; et al. Solution synthesis approach to colloidal cesium lead halide perovskite nanoplatelets with monolayer-level thickness control. *J. Am. Chem. Soc.* **2016**, *138*, 1010–1016. [[CrossRef](#)]
65. Do, M.; Kim, I.; Kolaczowski, M.A.; Kang, J.; Kamat, G.A.; Yuan, Z.; Barchi, N.S.; Wang, L.-W.; Liu, Y.; Jurow, M.J.; et al. Low-dimensional perovskite nanoplatelet synthesis using in situ photophysical monitoring to establish controlled growth. *Nanoscale* **2019**, *11*, 17262–17269. [[CrossRef](#)] [[PubMed](#)]
66. Li, J.; Zhang, H.; Wang, S.; Long, D.; Li, M.; Wang, D.; Zhang, T. Inter-conversion between different compounds of ternary Cs-Pb-Br system. *Materials* **2018**, *11*, 717. [[CrossRef](#)] [[PubMed](#)]
67. Li, M.; Zhang, X.; Dong, T.; Wang, P.; Matras-Postolek, K.; Yang, P. Evolution of morphology, phase composition and photoluminescence of cesium lead bromine nanocrystals with temperature and precursors. *J. Phys. Chem. C* **2018**, *122*, 28968–28976. [[CrossRef](#)]
68. Ji, Y.; Wang, M.; Yang, Z.; Ji, S.; Qiu, H. Nanowire-assisted self-assembly of one-dimensional nanocrystal superlattice chains. *J. Mater. Chem. C* **2019**, *7*, 8471–8476. [[CrossRef](#)]
69. Li, H.; Zhao, G.; Song, B.; Dong, W.; Han, G. Suppressing growth strategy on synthesizing stable and high-quality blue-emitting  $\text{CsPbBr}_3$  quantum dots. *ACS Appl. Opt. Mater.* **2023**, *1*, 1263–1271. [[CrossRef](#)]
70. Liang, Z.; Zhao, S.; Xu, Z.; Qiao, B.; Song, P.; Xu, X. Shape-controlled synthesis of all-inorganic  $\text{CsPbBr}_3$  perovskite nanocrystals with bright blue emission. *ACS Appl. Mater. Interfaces* **2016**, *8*, 28824–28830. [[CrossRef](#)]
71. Zhang, D.; Eaton, S.W.; Yu, Y.; Dou, L.; Yang, P. Solution-phase synthesis of cesium lead halide perovskite nanowires. *J. Am. Chem. Soc.* **2015**, *137*, 9230–9233. [[CrossRef](#)] [[PubMed](#)]
72. Bi, C.; Hu, J.; Yao, Z.; Lu, Y.; Binks, D.; Sui, M.; Tian, J. Self-assembled perovskite nanowire clusters for high luminance red light-emitting diodes. *Adv. Funct. Mater.* **2020**, *30*, 2005990. [[CrossRef](#)]

73. Tong, Y.; Bladt, E.; Ayguler, M.F.; Manzi, A.; Milowska, K.Z.; Hintermayr, V.A.; Docampo, P.; Bals, S.; Urban, A.S. Highly luminescent cesium lead halide perovskite nanocrystals with tunable composition and thickness by ultrasonication. *Angew. Chem.* **2016**, *55*, 13887–13892. [[CrossRef](#)]
74. Zhang, Z.; Liu, Y.; Geng, C.; Shi, S.; Zhang, X.; Bi, W.; Xu, S. Rapid synthesis of quantum-confined CsPbBr<sub>3</sub> perovskite nanowires using a microfluidic reactor. *Nanoscale* **2019**, *11*, 18790–18796. [[CrossRef](#)] [[PubMed](#)]
75. Yang, H.; Cai, T.; Dube, L.; Hills-Kimball, K.; Chen, O. Synthesis of ultrathin perovskite nanowires via a postsynthetic transformation reaction of zero-dimensional perovskite nanocrystals. *Cryst. Growth Des.* **2021**, *21*, 1924–1930. [[CrossRef](#)]
76. Fanizza, E.; Cascella, F.; Altamura, D.; Giannini, C.; Panniello, A.; Triggiani, L.; Panzarea, F.; Depalo, N.; Grisorio, R.; Suranna, G.P.; et al. Post-synthesis phase and shape evolution of CsPbBr<sub>3</sub> colloidal nanocrystals: The role of ligands. *Nano Res.* **2019**, *12*, 1155–1166. [[CrossRef](#)]
77. Paul, S.; Acharya, S. Postsynthesis transformation of halide perovskite nanocrystals. *ACS Energy Lett.* **2022**, *7*, 2136–2155. [[CrossRef](#)]
78. Aamir, M.; Adhikari, T.; Sher, M.; Khan, M.D.; Akhtar, J.; Nunzi, J.-M. Cesium lead halide perovskite nanostructures: Tunable morphology and halide composition. *Chem. Rec.* **2018**, *18*, 230–238. [[CrossRef](#)]
79. Yu, M.; Zhang, D.; Xu, Y.; Lin, J.; Yu, C.; Fang, Y.; Liu, Z.; Guo, Z.; Tang, C.; Huang, Y. Surface ligand engineering of CsPbBr<sub>3</sub> perovskite nanowires for high-performance photodetectors. *J. Colloid Interface Sci.* **2022**, *608*, 2367–2376. [[CrossRef](#)]
80. Imran, M.; Di Stasio, F.; Dang, Z.; Canale, C.; Khan, A.H.; Shamsi, J.; Brescia, R.; Prato, M.; Manna, L. Colloidal synthesis of strongly fluorescent CsPbBr<sub>3</sub> nanowires with width tunable down to the quantum confinement regime. *Chem. Mater.* **2016**, *28*, 6450–6454. [[CrossRef](#)]
81. Welyab, G.; Abebe, M.; Mani, D.; Thankappan, A.; Thomas, S.; Aga, A.G.; Kim, J.Y. All-inorganic CsPbBr<sub>3</sub> perovskite nanocrystals synthesized with olive oil and oleylamine at room temperature. *Micromachines* **2023**, *14*, 1332. [[CrossRef](#)] [[PubMed](#)]
82. Ghorri, A.; Midya, A.; Ray, S.K. Surfactant-induced anion exchange and morphological evolution for composition-controlled caesium lead halide perovskites with tunable optical properties. *ACS Omega* **2019**, *4*, 12948–12954. [[CrossRef](#)] [[PubMed](#)]
83. He, H.; Tang, B.; Ma, Y. Controlled synthesis of quantum confined CsPbBr<sub>3</sub> perovskite nanocrystals under ambient conditions. *Nanotechnology* **2018**, *29*, 055601. [[CrossRef](#)] [[PubMed](#)]
84. Hudait, B.; Dutta, S.K.; Patra, A.; Nasipuri, D.; Pradhan, N. Facets directed connecting perovskite nanocrystals. *J. Am. Chem. Soc.* **2020**, *142*, 7207–7217. [[CrossRef](#)]
85. Bekenstein, Y.; Koscher, B.A.; Eaton, S.W.; Yang, P.; Alivisatos, A.P. Highly luminescent colloidal nanoplates of perovskite cesium lead halide and their oriented assemblies. *J. Am. Chem. Soc.* **2015**, *137*, 16008–16011. [[CrossRef](#)]
86. Xiao, X.; Li, Y.; Xie, R.-J. Blue-emitting and self-assembled thinner perovskite CsPbBr<sub>3</sub> nanoplates: Synthesis and formation mechanism. *Nanoscale* **2020**, *12*, 9231–9239. [[CrossRef](#)]
87. Pramanik, A.; Sinha, S.S.; Gates, K.; Nie, J.; Han, F.X.; Ray, P.C. Light-induced wavelength dependent self assembly process for targeted synthesis of phase stable 1D nanobelts and 2D nanoplatelets of CsPbI<sub>3</sub> perovskites. *ACS Omega* **2023**, *8*, 13202–13212. [[CrossRef](#)]
88. Liu, J.; Song, K.; Shin, Y.; Liu, X.; Chen, J.; Yao, K.X.; Pan, J.; Yang, C.; Yin, J.; Xu, L.-J.; et al. Light-induced self-assembly of cubic CsPbBr<sub>3</sub> perovskite nanocrystals into nanowires. *Chem. Mater.* **2019**, *31*, 6642–6649. [[CrossRef](#)]
89. Li, H.; Lu, W.; Zhao, G.; Song, B.; Dong, W.; Han, G. Synthesis of size-controllable self-assembled CsPbBr<sub>3</sub> nanowires: Implications for photoemission with less recombination. *ACS Appl. Nano Mater.* **2022**, *5*, 5527–5534. [[CrossRef](#)]
90. Mehetor, S.K.; Ghosh, H.; Pradhan, N. Blue-emitting CsPbBr<sub>3</sub> perovskite quantum rods and their wide-area 2D self-assembly. *ACS Energy Lett.* **2019**, *4*, 1437–1442. [[CrossRef](#)]
91. Patra, B.K.; Agrawal, H.; Zheng, J.-Y.; Zha, X.; Travesset, A.; Garnett, E.C. Close-packed ultrasmooth self-assembled monolayer of CsPbBr<sub>3</sub> perovskite nanocubes. *ACS Appl. Mater. Interfaces* **2020**, *12*, 31764–31769. [[CrossRef](#)]
92. van der Burgt, J.S.; Geuchies, J.J.; van der Meer, B.; Vanrompay, H.; Zanaga, D.; Zhang, Y.; Albrecht, W.; Petukhov, A.V.; Filion, L.; Bals, S.; et al. Cuboidal supraparticles self-assembled from cubic CsPbBr<sub>3</sub> perovskite nanocrystals. *J. Phys. Chem. C* **2018**, *122*, 15706–15712. [[CrossRef](#)] [[PubMed](#)]
93. Li, H.; Liu, X.; Ying, Q.; Wang, C.; Jia, W.; Xing, X.; Yin, L.; Lu, Z.; Zhang, K.; Pan, Y.; et al. Self-assembly of perovskite CsPbBr<sub>3</sub> quantum dots driven by a photo-induced alkynyl homocoupling reaction. *Angew. Chem.* **2020**, *59*, 17207–17213. [[CrossRef](#)]
94. Pan, J.; Huang, H.; Zhao, W.; Lin, D.; Nie, Z.; Zhong, J.; Ma, L.; Zhang, X. Efficient and stable self-assembly blue-emitting CsPbBr<sub>3</sub> nanoplatelets with self-repaired surface defects. *ACS Appl. Nano Mater.* **2022**, *5*, 15062–15069. [[CrossRef](#)]
95. Mehetor, S.K.; Ghosh, H.; Pradhan, N. Acid-amine equilibria for formation and long-range self-organization of ultrathin CsPbBr<sub>3</sub> perovskite platelets. *J. Phys. Chem. Lett.* **2019**, *10*, 1300–1305. [[CrossRef](#)] [[PubMed](#)]
96. Kostopoulou, A.; Sygletou, M.; Brintakis, K.; Lappas, A.; Stratakis, E. Low-temperature benchtop-synthesis of all-inorganic perovskite nanowires. *Nanoscale* **2017**, *9*, 18202–18207. [[CrossRef](#)] [[PubMed](#)]
97. Li, H.; Lu, W.; Zhao, G.; Song, B.; Dong, W.; Han, G. Evolution and mechanism of cesium lead bromide nanostructures in oleylamine-rich system by hot-injection method. *Adv. Mater. Interfaces* **2023**, *10*, 2201916. [[CrossRef](#)]
98. Pan, J.; Li, X.; Gong, X.; Yin, J.; Zhou, D.; Sinatra, L.; Huang, R.; Liu, J.; Chen, J.; Dursun, I.; et al. Halogen vacancies enable ligand-assisted self-assembly of perovskite quantum dots into nanowires. *Angew. Chem.* **2019**, *131*, 16223–16227. [[CrossRef](#)]

99. Baranov, D.; Fieramosca, A.; Yang, R.X.; Polimeno, L.; Lerario, G.; Toso, S.; Giansante, C.; De Giorgi, M.; Tan, L.Z.; Sanvitto, D.; et al. Aging of self-assembled lead halide perovskite nanocrystal superlattices: Effects on photoluminescence and energy transfer. *ACS Nano* **2021**, *15*, 650–664. [[CrossRef](#)]
100. Pradhan, B.; Mushtaq, A.; Roy, D.; Sain, S.; Das, B.; Ghorai, U.K.; Pal, S.K.; Acharya, S. Postsynthesis spontaneous coalescence of mixed-halide perovskite nanocubes into phase-stable single-crystalline uniform luminescent nanowires. *J. Phys. Chem. Lett.* **2019**, *10*, 1805–1812. [[CrossRef](#)]
101. Soetan, N.; Erwin, W.R.; Tonigan, A.M.; Walker, D.G.; Bardhan, R. Solvent-assisted self-assembly of CsPbBr<sub>3</sub> perovskite nanocrystals into one-dimensional super-lattice. *J. Phys. Chem. C* **2017**, *121*, 18186–18194. [[CrossRef](#)]
102. Chen, Y.-L.; Hu, Y.-H.; Ma, L.; Zhang, X.-Y.; Zhao, N.-X.; Yang, X.; Zhang, Y.-S.; Gu, Y.-L.; Xu, S.-L.; Dong, X.; et al. Self-assembled CsPbBr<sub>3</sub> quantum dots with wavelength-tunable photoluminescence for efficient active jamming. *Nanoscale* **2022**, *14*, 17900–17907. [[CrossRef](#)]
103. Leng, J.; Wang, T.; Zhao, X.; Ong, E.W.Y.; Zhu, B.; de Andrew Ng, J.; Wong, Y.-C.; Khoo, K.H.; Tamada, K.; Tan, Z.-K. Thermodynamic control in the synthesis of quantum-confined blue-emitting CsPbBr<sub>3</sub> perovskite nanostrips. *J. Phys. Chem. Lett.* **2020**, *11*, 2036–2043. [[CrossRef](#)] [[PubMed](#)]
104. Zhang, L.; Zhang, Y.; He, W.; Peng, H.; Dai, Q. CsPbBr<sub>3</sub> perovskite nanowires and their optical properties. *Opt. Mater.* **2020**, *109*, 110399. [[CrossRef](#)]
105. Zhou, Z.-R.; Liao, Z.-H.; Wang, F. Shape-controlled synthesis of one-dimensional cesium lead halide perovskite nanocrystals: Methods and advances. *J. Mater. Chem. C* **2023**, *11*, 3409–3427. [[CrossRef](#)]
106. Krajewska, C.J.; Kaplan, A.E.K.; Kick, M.; Berkinsky, D.B.; Zhu, H.; Sverko, T.; Voorhis, T.V.; Bawendi, M.G. Controlled assembly and anomalous thermal expansion of ultrathin cesium lead bromide nanoplatelets. *Nano Lett.* **2023**, *23*, 2148–2157. [[CrossRef](#)]
107. Dang, Z.; Dhanabalan, B.; Castelli, A.; Dhall, R.; Bustillo, K.C.; Marchelli, D.; Spirito, D.; Petralanda, U.; Shamsi, J.; Manna, L.; et al. Temperature-driven transformation of CsPbBr<sub>3</sub> nanoplatelets into mosaic nanotiles in solution through self-assembly. *Nano Lett.* **2020**, *20*, 1808–1818. [[CrossRef](#)]
108. Montanarella, F.; Akkerman, Q.A.; Bonatz, D.; van der Sluijs, M.M.; van der Bok, J.C.; Prins, P.T.; Aebli, M.; Mews, A.; Vanmaekelbergh, D.; Kovalenko, M.V. Growth and self-assembly of CsPbBr<sub>3</sub> nanocrystals in the TOPO/PbBr<sub>2</sub> synthesis as seen with X-ray scattering. *Nano Lett.* **2023**, *23*, 667–676. [[CrossRef](#)]
109. Liu, Z.; Bekenstein, Y.; Ye, X.; Nguyen, S.C.; Swabeck, J.; Zhang, D.; Lee, S.-T.; Yang, P.; Ma, W.; Alivisatos, A.P. Ligand mediated transformation of cesium lead bromide perovskite nanocrystals to lead depleted Cs<sub>4</sub>PbBr<sub>6</sub> nanocrystals. *J. Am. Chem. Soc.* **2017**, *139*, 5309–5312. [[CrossRef](#)]
110. Udayabhaskararao, T.; Houben, L.; Cohen, H.; Menahem, M.; Pinkas, I.; Avram, L.; Wolf, T.; Teitelboim, A.; Leskes, M.; Yaffe, O.; et al. A mechanistic study of phase transformation in perovskite nanocrystals driven by ligand Passivation. *Chem. Mater.* **2018**, *30*, 84–93. [[CrossRef](#)]
111. Dahl, J.C.; Wang, X.; Huang, X.; Chan, E.M.; Alivisatos, A.P. Elucidating the weakly reversible Cs-Pb-Br perovskite nanocrystal reaction network with high-throughput maps and transformations. *J. Am. Chem. Soc.* **2020**, *142*, 11915. [[CrossRef](#)] [[PubMed](#)]
112. Bao, Z.; Chiu, H.-D.; Wang, W.; Su, Q.; Yamada, T.; Chang, Y.-C.; Chen, S.; Kanemitsu, Y.; Chung, R.-J.; Liu, R.-S. Highly luminescent CsPbBr<sub>3</sub>@Cs<sub>4</sub>PbBr<sub>6</sub> nanocrystals and their application in electroluminescent emitters. *J. Phys. Chem. Lett.* **2020**, *11*, 10196–10202. [[CrossRef](#)] [[PubMed](#)]
113. Qin, Z.; Dai, S.; Hadjiev, V.G.; Wang, C.; Xie, L.; Ni, Y.; Wu, C.; Yang, G.; Chen, S.; Deng, L.; et al. Revealing the origin of luminescence center in 0D Cs<sub>4</sub>PbBr<sub>6</sub> perovskite. *Chem. Mater.* **2019**, *31*, 9098–9104. [[CrossRef](#)]
114. Ray, A.; Maggioni, D.; Baranov, D.; Dang, Z.; Prato, M.; Akkerman, Q.A.; Goldoni, L.; Caneva, E.; Manna, L.; Abdelhady, A.L. Green-emitting powders of zero-dimensional Cs<sub>4</sub>PbBr<sub>6</sub>: Delineating the intricacies of the synthesis and the origin of photoluminescence. *Chem. Mater.* **2019**, *31*, 7761–7769. [[CrossRef](#)]
115. Jing, Q.; Xu, Y.; Su, Y.; Xing, X.; Lu, Z. A systematic study of the synthesis of cesium lead halide nanocrystals: Does Cs<sub>4</sub>PbBr<sub>6</sub> or CsPbBr<sub>3</sub> form? *Nanoscale* **2019**, *11*, 1784–1789. [[CrossRef](#)]
116. Cho, J.; Banerjee, S. Ligand-directed stabilization of ternary phases: Synthetic control of structural dimensionality in solution-grown cesium lead bromide nanocrystals. *Chem. Mater.* **2018**, *30*, 6144–6155. [[CrossRef](#)]
117. Li, Y.; Huang, H.; Xiong, Y.; Kershaw, S.V.; Rogach, A.L. Revealing the formation mechanism of CsPbBr<sub>3</sub> perovskite nanocrystals produced via a slowed-down microwave-assisted synthesis. *Angew. Chem.* **2018**, *57*, 5833–5837. [[CrossRef](#)]
118. Xiao, M.; Hao, M.; Lyu, M.; Moore, E.G.; Zhang, C.; Zhang, C.; Luo, B.; Hou, J.; Lipton-Duffin, J.; Wang, L. Surface ligands stabilized lead halide perovskite quantum dot photocatalyst for visible light-driven hydrogen generation. *Adv. Funct. Mater.* **2019**, *29*, 1905683. [[CrossRef](#)]
119. Chen, L.-C.; Tien, C.-H.; Tseng, P.-W.; Tseng, Z.-L.; Huang, W.-L.; Xu, Y.-X.; Kuo, H.-C. Effect of washing solvents on the properties of air-synthesized perovskite CsPbBr<sub>3</sub> quantum dots for quantum dot-based light-emitting devices. *IEEE Access* **2020**, *8*, 159415–159423. [[CrossRef](#)]
120. Li, F.; Lin, F.; Huang, Y.; Cai, Z.; Qiu, L.; Zhu, Y.; Wang, Y.; Chen, X. Bromobenzene aliphatic nucleophilic substitution guided controllable and reproducible synthesis of high quality cesium lead bromide perovskite nanocrystals. *Inorg. Chem. Front.* **2019**, *6*, 3577–3582. [[CrossRef](#)]

121. Quarta, D.; Imran, M.; Capodilupo, A.-L.; Petralanda, U.; van Beek, B.; De Angelis, F.; Manna, L.; Infante, I.; De Trizio, L.; Giansante, C. Stable ligand coordination at the surface of colloidal CsPbBr<sub>3</sub> nanocrystals. *J. Phys. Chem. Lett.* **2019**, *10*, 3715–3726. [[CrossRef](#)] [[PubMed](#)]
122. Dong, Y.; Zhao, Y.; Zhang, S.; Dai, Y.; Liu, L.; Li, Y.; Chen, Q. Recent advances toward practical use of halide perovskite nanocrystals. *J. Mater. Chem. A* **2018**, *6*, 21729–21746. [[CrossRef](#)]
123. Yang, D.; Cao, M.; Zhong, Q.; Li, P.; Zhang, X.; Zhang, Q. All-inorganic cesium lead halide perovskite nanocrystals: Synthesis, surface engineering and applications. *J. Mater. Chem. C* **2019**, *7*, 757–789. [[CrossRef](#)]
124. McGrath, F.; Ghorpade, U.V.; Ryan, K.M. Synthesis and dimensional control of CsPbBr<sub>3</sub> perovskite nanocrystals using phosphorous based ligands. *J. Chem. Phys.* **2020**, *152*, 174702. [[CrossRef](#)] [[PubMed](#)]
125. Fiuza-Maneiro, N.; Sun, K.; Lopez-Fernandez, I.; Gomez-Grana, S.; Muller-Buschbaum, P.; Polavarapu, L. Ligand chemistry of inorganic lead halide perovskite nanocrystals. *ACS Energy Lett.* **2023**, *8*, 1152–1191. [[CrossRef](#)]
126. Smock, S.R.; Williams, T.J.; Brutchey, R.L. Quantifying the thermodynamics of ligand binding to CsPbBr<sub>3</sub> quantum dots. *Angew. Chem.* **2018**, *57*, 11711–11715. [[CrossRef](#)]
127. Zaccaria, F.; Zhang, B.; Goldoni, L.; Imran, M.; Zito, J.; van Beek, B.; Lauciello, S.; De Trizio, L.; Manna, L.; Infante, I. The reactivity of CsPbBr<sub>3</sub> nanocrystals toward acid/base ligands. *ACS Nano* **2022**, *16*, 1444–1455. [[CrossRef](#)]
128. Akhil, S.; Dutt, V.; Mishra, N. Bromopropane as a novel bromine precursor for the completely amine free colloidal synthesis of ultrastable and highly luminescent green-emitting cesium lead bromide (CsPbBr<sub>3</sub>) perovskite nanocrystals. *Nanoscale* **2021**, *13*, 13142–13151. [[CrossRef](#)]
129. Akhil, S.; Biswas, S.; Palabathuni, M.; Singh, R.; Mishra, N. Amine-free synthetic route: An emerging approach to making high-quality perovskite nanocrystals for futuristic applications. *J. Phys. Chem. Lett.* **2022**, *13*, 9480–9493. [[CrossRef](#)]
130. Akhil, S.; Dutt, V.G.V.; Singh, R.; Mishra, N. Surface-state-mediated interfacial hole transfer dynamics between CsPbBr<sub>3</sub> perovskite nanocrystals and phenothiazine redox couple. *J. Phys. Chem. C* **2021**, *125*, 22133–22141. [[CrossRef](#)]
131. Chen, W.-C.; Fang, Y.-H.; Chen, L.-G.; Liang, F.-C.; Yan, Z.-L.; Ebe, H.; Takahashi, Y.; Chiba, T.; Kido, J.; Kuo, C.-C. High luminescence and external quantum efficiency in perovskite quantum-dots light-emitting diodes featuring bilateral affinity to silver and short alkyl ligands. *Chem. Eng. J.* **2021**, *414*, 128866. [[CrossRef](#)]
132. Zheng, W.; Wan, Q.; Liu, M.; Zhang, Q.; Zhang, C.; Yan, R.; Feng, X.; Kong, L.; Li, L. CsPbBr<sub>3</sub> nanocrystal light-emitting diodes with efficiency up to 13.4% achieved by careful surface engineering and device engineering. *J. Phys. Chem. C* **2021**, *125*, 3110–3118. [[CrossRef](#)]
133. Chiba, T.; Hoshi, K.; Pu, Y.-J.; Takeda, Y.; Hayashi, Y.; Ohisa, S.; Kawata, S.; Kido, J. High-efficiency perovskite quantum-dot light-emitting devices by effective washing process and interfacial energy level alignment. *ACS Appl. Mater. Interfaces* **2017**, *9*, 18054–18060. [[CrossRef](#)] [[PubMed](#)]
134. Zhang, Y.; Hou, G.; Wu, Y.; Chen, M.; Dai, Y.; Liu, S.; Zhao, Q.; Lin, H.; Fang, J.; Jing, C.; et al. Surface reconstruction of CsPbBr<sub>3</sub> nanocrystals by the ligand engineering approach for achieving high quantum yield and improved stability. *Langmuir* **2023**, *39*, 6222–6230. [[CrossRef](#)]
135. Abiodun, S.L.; Pellechia, P.J.; Greytak, A.B. Effective purification of CsPbBr<sub>3</sub> nanocrystals with high quantum yield and high colloidal stability via gel permeation chromatography. *J. Phys. Chem. C* **2021**, *125*, 3463–3471. [[CrossRef](#)]
136. Abiodun, S.L.; Gee, M.Y.; Greytak, A.B. Combined NMR and isothermal titration calorimetry investigation resolves conditions for ligand exchange and phase transformation in CsPbBr<sub>3</sub> nanocrystals. *J. Phys. Chem. C* **2021**, *125*, 17897–17905. [[CrossRef](#)]
137. Balakrishnan, S.K.; Kamat, P.V. Ligand assisted transformation of cubic CsPbBr<sub>3</sub> nanocrystals into two-dimensional CsPb<sub>2</sub>Br<sub>5</sub> nanosheets. *Chem. Mater.* **2018**, *20*, 74–78. [[CrossRef](#)]
138. Akhil, S.; Dutt, V.G.; Singh, R.; Mishra, N. Post-synthesis treatment with lead bromide for obtaining near-unity photoluminescence quantum yield and ultra-stable amine-free CsPbBr<sub>3</sub> perovskite nanocrystals. *J. Phys. Chem. C* **2022**, *126*, 10742–10751. [[CrossRef](#)]
139. VanOrman, Z.A.; Weiss, R.; Medina, M.; Nienhaus, L. Scratching the surface: Passivating perovskite nanocrystals for future device integration. *J. Phys. Chem. Lett.* **2022**, *13*, 982–990. [[CrossRef](#)]
140. Krieg, F.; Ochsenbein, S.T.; Yakunin, S.; ten Brinck, S.; Aellen, P.; Suess, A.; Clerc, B.; Guggisberg, D.; Nazarenko, O.; Shynkarenko, Y.; et al. Colloidal CsPbX<sub>3</sub> (X = Cl, Br, I) nanocrystals 2.0: Zwitterionic capping ligands for improved durability and stability. *ACS Energy Lett.* **2018**, *3*, 641–646. [[CrossRef](#)]
141. Wang, C.; Malinoski, A.; Yuan, J.; Hu, G. A surface engineering approach for promoting dexter energy transfer from lead halide perovskite nanocrystals. *J. Phys. Chem. C* **2023**, *127*, 1135–1144. [[CrossRef](#)]
142. Mei, X.; He, K.; Zhuang, R.; Yu, M.; Hua, Y.; Zhang, X. Stabilizing dynamic surface of highly luminescent perovskite quantum dots for light-emitting diodes. *Chem. Eng. J.* **2023**, *453*, 139909. [[CrossRef](#)]
143. Kreig, F.; Ong, Q.K.; Burian, M.; Raino, G.; Naumenko, D.; Amenitsch, H.; Suess, A.; Grotevent, M.J.; Krumeich, F.; Bodnarchuk, M.I.; et al. Stable ultraconcentrated and ultradilute colloids of CsPbX<sub>3</sub> (X = Cl, Br) nanocrystals using natural lecithin as a capping ligand. *J. Am. Chem. Soc.* **2019**, *141*, 19839–19849. [[CrossRef](#)] [[PubMed](#)]
144. Grisorio, R.; Fasulo, F.; Munoz-Garcia, A.B.; Pavone, M.; Conelli, D.; Fanizza, E.; Striccoli, M.; Allegretta, I.; Terzano, R.; Margiotta, N.; et al. In situ formation of zwitterionic ligands: Changing the passivation paradigms of CsPbBr<sub>3</sub> nanocrystals. *Nano Lett.* **2022**, *22*, 4437–4444. [[CrossRef](#)] [[PubMed](#)]

145. Montanarella, F.; McCall, K.M.; Sakhatskyi, K.; Yakunin, S.; Trtik, P.; Bernasconi, C.; Cherniukh, I.; Mannes, D.; Bodnarchuk, M.I.; Strobl, M.; et al. Highly concentrated, zwitterionic ligand-capped  $\text{Mn}^{2+}$ : $\text{CsPb}(\text{Br}_x\text{Cl}_{1-x})_3$  nanocrystals as bright scintillators for fast neutron imaging. *ACS Energy Lett.* **2021**, *6*, 4365–4373. [[CrossRef](#)]
146. Lee, A.-Y.; Kim, J.; Lee, D.; Song, M.H. Efficient and stable perovskite nanocrystal light-emitting diodes with sulfobetaine-based ligand treatment. *ACS Appl. Electron. Mater.* **2023**, *5*, 5325–5331. [[CrossRef](#)]
147. Guo, S.; Liu, H.; He, H.; Wang, W.; Jiang, L.; Xiong, X.; Wang, L. Eco-friendly strategy to improve durability and stability of zwitterionic capping ligand colloidal  $\text{CsPbBr}_3$  nanocrystals. *Langmuir* **2020**, *36*, 6775–6781. [[CrossRef](#)]
148. Manoli, A.; Papagiorgis, P.; Sergides, M.; Bernasconi, C.; Athanasiou, M.; Pozov, S.; Choulis, S.A.; Bodnarchuk, M.I.; Kovalenko, M.V.; Othonos, A.; et al. Surface functionalization of  $\text{CsPbBr}_3$  nanocrystals for photonic applications. *ACS Appl. Nano Mater.* **2021**, *4*, 5084–5097. [[CrossRef](#)]
149. Shcherbakov-Wu, W.; Sercel, P.C.; Krieg, F.; Kovalenko, M.V.; Tisdale, W.A. Temperature-independent dielectric constant in  $\text{CsPbBr}_3$  nanocrystals revealed by linear absorption spectroscopy. *J. Phys. Chem. Lett.* **2021**, *12*, 8088–8095. [[CrossRef](#)]
150. Wang, S.; Du, L.; Jin, Z.; Xin, Y.; Mattoussi, H. Enhanced stabilization and easy phase transfer of  $\text{CsPbBr}_3$  perovskite quantum dots promoted by high-affinity polyzwitterionic ligands. *J. Am. Chem. Soc.* **2020**, *142*, 12669–12680. [[CrossRef](#)]
151. Jin, X.; Ma, K.; Gao, H. Tunable luminescence and enhanced polar solvent resistance of perovskite nanocrystals achieved by surface-initiated photopolymerization. *J. Am. Chem. Soc.* **2022**, *144*, 20411–20420. [[CrossRef](#)] [[PubMed](#)]
152. Jin, H.; Park, G.Y.; Kim, M.K.; Cha, J.; Ham, D.S.; Kim, M. Eco-friendly solvent-processible and highly luminescent perovskite nanocrystals with polymer zwitterions for air-stable optoelectronics. *Chem. Eng. J.* **2023**, *459*, 141531. [[CrossRef](#)]
153. Noh, S.H.; Jeong, W.; Lee, K.H.; Yang, H.S.; Suh, E.H.; Jung, J.; Park, S.C.; Lee, D.; Jung, I.H.; Jeong, Y.J.; et al. Photocrosslinkable zwitterionic ligands for perovskite nanocrystals: Self-assembly and high-resolution direct patterning. *Adv. Funct. Mater.* **2023**, *33*, 2304004. [[CrossRef](#)]
154. Zhang, M.; Zhang, J.; Zhao, G.; Wang, G.; Liu, P.; Li, H.; Hou, X.; Qiang, P.; Yang, Y.; Su, Q.; et al. Efficient blue  $\text{CsPbBr}_3$  perovskite nanocrystals synthesis with the assistance of zwitterionic straight chain amino acids. *Colloids Surf. A Physicochem. Eng. Asp.* **2023**, *673*, 131793. [[CrossRef](#)]
155. Cohen, T.A.; Huang, Y.; Bricker, N.A.; Juhl, C.S.; Milstein, T.J.; MacKenzie, J.D.; Luscombe, C.K.; Gamelin, D.R. Modular zwitterion-functionalized poly(isopropyl methacrylate) polymers for hosting luminescent lead halide perovskite nanocrystals. *Chem. Mater.* **2021**, *33*, 3779–3790. [[CrossRef](#)]
156. Kirsch, C.; Naujoks, T.; Haizmann, P.; Frech, P.; Peisert, H.; Chasse, T.; Brutting, W.; Scheele, M. Zwitterionic carbazole ligands enhance the stability and performance of perovskite nanocrystals in light-emitting diode. *ACS Appl. Mater. Interfaces* **2023**, *15*, 32744–32752. [[CrossRef](#)]
157. Zhu, H.; Kick, M.; Ginterseder, M.; Krajewska, C.J.; Sverko, T.; Li, R.; Lu, R.; Shih, M.-C.; Voorhis, T.V.; Bawendi, M.G. Synthesis of zwitterionic  $\text{CsPbBr}_3$  nanocrystals with controlled anisotropy using surface-selective ligand pairs. *Adv. Mater.* **2023**, *35*, 2304069. [[CrossRef](#)]
158. Xie, Q.; Wu, D.; Wang, X.; Li, Y.; Fang, F.; Wang, Z.; Ma, Y.; Su, M.; Peng, S.; Liu, H.; et al. Branched capping ligands improve the stability of cesium lead halide ( $\text{CsPbBr}_3$ ) perovskite quantum dots. *J. Mater. Chem. C* **2019**, *7*, 11251–11257. [[CrossRef](#)]
159. Wang, X.; Zhu, S.; Fu, J.; Li, X.; Zhao, X.; Jiang, H.; Lv, G.; Li, P.; Li, J.; Zhang, W.-H.; et al. Hybrid ligand polymerization for weakly confined lead halide perovskite quantum dots. *ACS Appl. Mater. Interfaces* **2023**, *15*, 20208–20218. [[CrossRef](#)]
160. Hou, S.; Guo, Y.; Tang, Y.; Quan, Q. Synthesis and stabilization of colloidal perovskite nanocrystals by multidentate polymer micelles. *ACS Appl. Mater. Interfaces* **2017**, *9*, 18417–18422. [[CrossRef](#)]
161. Sanjayan, C.G.; Jyothi, M.S.; Sakar, M.; Balakrishna, R.G. Multidentate ligand approach for conjugation of perovskite quantum dots to biomolecules. *J. Colloid Interface Sci.* **2021**, *603*, 758–770. [[CrossRef](#)] [[PubMed](#)]
162. Chen, J.; Jia, D.; Qiu, J.; Zhuang, R.; Hua, Y.; Zhang, X. Multidentate passivation crosslinking perovskite quantum dots for efficient solar cells. *Nano Energy* **2022**, *96*, 107140. [[CrossRef](#)]
163. Jin, X.; Ma, K.; Chakkamalayath, J.; Morsby, J.; Gao, H. In situ photocatalyzed polymerization to stabilize perovskite nanocrystals in protic solvents. *ACS Energy Lett.* **2022**, *7*, 610–616. [[CrossRef](#)]
164. Pan, Q.; Hu, J.; Fu, J.; Lin, Y.; Zou, C.; Di, D.; Wang, Y.; Zhang, Q.; Cao, M. Ultrahigh stability of perovskite nanocrystals by using semiconducting molecular species for displays. *ACS Nano* **2022**, *16*, 12253–12261. [[CrossRef](#)]
165. Yin, W.; Li, M.; Dong, W.; Luo, Z.; Li, Y.; Qian, J.; Zhang, J.; Zhang, W.; Zhang, Y.; Kershaw, S.V.; et al. Multidentate ligand polyethyleneimine enables bright color-saturated blue light-emitting diodes based on  $\text{CsPbBr}_3$  nanoplatelets. *ACS Energy Lett.* **2021**, *6*, 477–484. [[CrossRef](#)]
166. Wang, S.; Du, L.; Donmez, S.; Xin, Y.; Mattoussi, H. Polysalt ligands achieve higher quantum yield and improved colloidal stability for  $\text{CsPbBr}_3$  quantum dots. *Nanoscale* **2021**, *13*, 16705–16718. [[CrossRef](#)]
167. Wang, S.; Wang, W.; Donmez, S.; Xin, Y.; Mattoussi, H. Engineering highly fluorescent and colloidally stable blue-emitting  $\text{CsPbBr}_3$  nanoplatelets using polysalt/ $\text{PbBr}_2$  ligands. *Chem. Mater.* **2022**, *34*, 4924–4936. [[CrossRef](#)]
168. Malinoski, A.; Hu, G.; Wang, C. Strong bidentate coordination for surface passivation and ligand-shell engineering of lead halide perovskite nanocrystals in the strongly quantum-confined regime. *J. Phys. Chem. C* **2021**, *125*, 24521–24530. [[CrossRef](#)]
169. Yin, W.; Li, M.; Dong, W.; Zhang, X.; Zheng, W. Overcoming the ambient manufacturability-performance bottleneck in perovskite nanocrystal emitters for efficient light-emitting diodes. *Angew. Chem.* **2023**, *62*, e202303462. [[CrossRef](#)]

170. Zhang, J.; Shen, W.; Chen, S.; Zhang, Z.; Cai, B.; Qiu, Y.; Jiang, J.; He, Y.; Nan, M.; Chen, Y.; et al. Multidentate ligand-passivated CsPbI<sub>3</sub> perovskite nanocrystals for stable and efficient red-light-emitting diodes. *J. Phys. Chem. Lett.* **2023**, *14*, 6639–6646. [[CrossRef](#)]
171. Zeng, Q.; Zhang, X.; Bing, Q.; Xiong, Y.; Yang, F.; Liu, H.; Liu, J.-Y.; Zhang, H.; Zheng, W.; Rogach, A.L.; et al. Surface stabilization of colloidal perovskite nanocrystals via multi-amine chelating ligands. *ACS Energy Lett.* **2022**, *7*, 1963–1970. [[CrossRef](#)]
172. Yuan, Y.; Zhu, H.; Hills-Kimball, K.; Cai, T.; Shi, W.; Wei, Z.; Yang, H.; Candler, Y.; Wang, P.; He, J.; et al. Stereoselective C-C oxidative coupling reactions photocatalyzed by zwitterionic ligand capped CsPbBr<sub>3</sub> perovskite quantum dots. *Angew. Chem.* **2020**, *59*, 22563–22569. [[CrossRef](#)] [[PubMed](#)]
173. Ye, J.; Byranvand, M.M.; Martinez, C.O.; Hoye, R.L.Z.; Saliba, M.; Polavarapu, L. Defect passivation in lead-halide perovskite nanocrystals and thin films: Toward efficient LEDs and solar cells. *Angew. Chem.* **2021**, *133*, 21804–21828. [[CrossRef](#)]
174. Liu, M.; Matuhina, A.; Zhang, H.; Vivo, P. Advances in the stability of halide perovskite nanocrystals. *Materials* **2019**, *12*, 3733. [[CrossRef](#)]

**Disclaimer/Publisher's Note:** The statements, opinions and data contained in all publications are solely those of the individual author(s) and contributor(s) and not of MDPI and/or the editor(s). MDPI and/or the editor(s) disclaim responsibility for any injury to people or property resulting from any ideas, methods, instructions or products referred to in the content.